Dual Quaternion Based Fault-tolerant Control for Spacecraft Tracking with Finite-time Convergence

Hongyang Dong, Qinglei Hu, Michael I. Friswell, and Guangfu Ma

***Abstract*—Results are presented for a study of dual quaternion based fault-tolerant control for spacecraft tracking. First, a six degrees of freedom Lagrange-like model with a dual-quaternion-based description is employed to describe the relative coupled motion of a target-pursuer spacecraft formation. Then a novel fault-tolerant control method is proposed to enable the pursuer to track the attitude and position of the target even though its actuators have multiple faults. Furthermore, based on a novel time-varying sliding manifold, finite-time stability feature of the closed-loop system is theoretically guaranteed, and the convergence time of the system is given explicitly. Multiple-task capability of the proposed control law is further demonstrated in the presence of disturbances and parametric uncertainties. Finally, numerical simulations of the proposed method are presented to demonstrate the effectiveness and kinds of advantages of the proposed controller.**

***Index Terms*—fault-tolerant, finite-time, dual quaternion, spacecraft.**

I. Introduction

SPACECRAFT tracking [1-4] is one of the most important research areas of spacecraft control, which has been identified by the USA's advanced space transportation plan (ASTP) as one of the key technologies of multi-spacecraft tasks due to its crucial application in space surveillance, rendezvous and docking, and so on. In the process of spacecraft tracking, accurate mathematical models and control algorithms are required for the relative attitude and orbit motion between two spacecraft, namely a pursuer and a target. Kawano *et al.* [5] presented a tracking control test of the Engineering Test Satellite-VII. Wang *et al.* [6] applied the target-pursuer strategy to spacecraft formation, even in the presence of actuator saturation. An architecture for the multi-agent coordination system, including the target-pursuer strategy, and agent behavioral and virtual-structure approaches, was proposed in Ref. [7]. A schedule for the online generation of safe, fuel-optimized rendezvous trajectories was presented in Ref. [8]. Der-Ren *et al.* [9] introduced solutions for the problem of orbital rendezvous, and the issues considered included minimum fuel, fixed time, and path constraints.

In many on-orbit spacecraft formation missions, such as refueling, monitoring and on-orbit assembly, the pursuer spacecraft is required to track both the time-varying relative position and the reference attitude trajectories accurately and synchronously. For spacecraft formations, a controller based on a six degrees-of-freedom (6-DOF) model has significant advantages over a controller designed using a traditional 3-DOF separated model, and can be deduced in a much more compact form. Over recent years, studies about 6-DOF controller design for spacecraft formations have aroused general interest. An integrated position and attitude control for spacecraft final docking with a non-cooperative controller was proposed in Ref. [10]. Lv *et al.* [11] introduced a 6-DOF synchronized controller for spacecraft formation flying in the presence of input constraints and parameter uncertainties. Compared to other description methods, dual quaternions have been widely used recently due to their clear physical meaning and natural representation. Furthermore, the dual quaternion description takes into account the coupling between the rotation and translation automatically. Wang *et al.* [12] presented a 6-DOF model for spacecraft with a dual-number-based description, and then proposed sliding mode based finite-time control laws. A further adaptive robust control method based on this model was presented in Ref. [13].

Safety is the most fundamental and crucial requirement for spacecraft; if an actuator has an uncontrollable failure during the tracking process, it may cause huge economic losses. Some data [14] shows that over half of the task failures are related to actuator faults, and for this case, the fault-tolerant ability of controllers is very important and has received widespread attention. An indirect approach to spacecraft attitude fault-tolerant control for limited thrust was presented in Ref. [15]. Xiao *et al.* [16] introduced an adaptive robust control law for the spacecraft attitude tracking problem with actuator faults and saturation. Schetter *et al.* [17] proposed a multiple agent-based fault tolerance algorithm for satellite formation flying. Lee *et al.* [18] employed finite-time sliding mode control, and introduced a fault-tolerant attitude control scheme for satellites.

This paragraph of the first footnote will contain the date on which you submitted your paper for review. It will also contain support information, including sponsor and financial support acknowledgment. For example, "This work was supported in part by the U.S. Department of Commerce under Grant BS123456".

H. Dong is with the Department of Control Science and Technology, Harbin Institute of Technology, Harbin, 150001, China (email: donghongyang91@gmail.com)

Q. Hu is with the School of Automation Science and Electrical Engineering, Beihang University, Beijing, 100191, China (email: huql_buaa@buaa.edu.cn)

M. I. Friswell is with the College of Engineering, Swansea University Bay Campus, Swansea SA1 8EN, UK (email: m.i.friswell@swansea.ac.uk)

G. Ma is with the Department of Control Science and Technology, Harbin Institute of Technology, Harbin, 150001, China (email: magf@hit.edu.cn)

However, the fault-tolerant methods applied to fully coupled models of spacecraft are very conservative. Furthermore, the questions not merely consider 6-DOF synchronous control and fault-tolerant control, but also some other engineering requirements such as finite-time control, still remain open issues. In this paper, the 6-DOF coordinated tracking problem of spacecraft is considered. Specifically, a Lagrange-like dual-quaternion-based model is employed to describe the proximity operations between the two spacecraft (namely the target and the pursuer). Then, based on this structure and combined with the global sliding mode method [19, 20], a novel adaptive fault-tolerant control law is proposed to enable the pursuer to track the expected attitude and position of the target, even in the presence of multiple actuators faults, parameter uncertainties, and external disturbances. Furthermore, by introducing a novel nonlinear function into the sliding manifold, the tracking errors can be theoretically guaranteed to converge to zero in finite time, and this finite time is designed and expressed explicitly. The paper is organized as follows: an introduction about dual quaternions is given in Section 2, and then the 6-DOF coupled model used in this paper is presented in Section 3. In Section 4, the time-varying sliding manifold and the fault-tolerant finite-time controller are designed. Numerical simulation results are given in Section 5 to demonstrate the effectiveness of the controller. Finally, the paper ends with some conclusions.

II. Dual Numbers and Dual Quaternions

A. Dual Numbers and Dual Vectors

The concept of dual numbers and dual vectors was first proposed by Clifford [21], and then improved by Study [22]. Throughout this paper, the superscript $\hat{*}$ denotes the corresponding variable or constant is a dual variable or constant. The definition of a dual number is given by

$$\hat{a} = a + \varepsilon a^{\circ} \tag{1}$$

where $a, a^{\circ} \in \mathbb{R}$ are called the real part and the dual part of the dual number $\hat{a}$ respectively, and ε is called the dual unit which satisfies the conditions:

$$\varepsilon^2 = 0 \ \text{ and } \ \varepsilon \neq 0 \tag{2}$$

Dual vectors and dual matrices are classes of special vectors and matrices whose elements are dual numbers. Hence

$$\hat{\boldsymbol{a}} = \boldsymbol{a} + \varepsilon \boldsymbol{a}^{\circ} \tag{3}$$

$$\hat{\boldsymbol{A}} = \boldsymbol{A} + \varepsilon \boldsymbol{A}^{\circ} \tag{4}$$

where $\boldsymbol{a}, \boldsymbol{a}^{\circ} \in \mathbb{R}^n$ are real vectors and $\boldsymbol{A}, \boldsymbol{A}^{\circ} \in \mathbb{R}^{n\times n}$ are real matrices. Some common operations of dual numbers, vectors and matrices used in this paper are given below.

$$\hat{\boldsymbol{a}} \pm \hat{\boldsymbol{b}} = (\boldsymbol{a} + \varepsilon \boldsymbol{a}^{\circ}) \pm (\boldsymbol{b} + \varepsilon \boldsymbol{b}^{\circ}) = (\boldsymbol{a} \pm \boldsymbol{b}) + \varepsilon(\boldsymbol{a}^{\circ} \pm \boldsymbol{b}^{\circ}) \tag{5}$$

$$\hat{\boldsymbol{a}}^{\mathrm{T}} = \boldsymbol{a}^{\mathrm{T}} + \boldsymbol{a}^{\circ \mathrm{T}} \tag{6}$$

$$\boldsymbol{H}\hat{\boldsymbol{a}} = \boldsymbol{H}(\boldsymbol{a} + \varepsilon \boldsymbol{a}^{o}) = \boldsymbol{H}\boldsymbol{a} + \varepsilon \boldsymbol{H}\boldsymbol{a}^{o} \tag{7}$$

$$\hat{\boldsymbol{a}}\hat{\boldsymbol{b}} = \boldsymbol{a}\boldsymbol{b} + \varepsilon(\boldsymbol{a}\boldsymbol{b}^{\circ} + \boldsymbol{a}^{\circ}\boldsymbol{b}) \tag{8}$$

$$\hat{\boldsymbol{A}}\hat{\boldsymbol{a}} = \boldsymbol{A}\boldsymbol{a} + \varepsilon(\boldsymbol{A}\boldsymbol{a}^{\circ} + \boldsymbol{A}^{\circ}\boldsymbol{a}) \tag{9}$$

$$\hat{\boldsymbol{a}} \times \hat{\boldsymbol{b}} = \boldsymbol{a} \times \boldsymbol{b} + \varepsilon(\boldsymbol{a} \times \boldsymbol{b}^{\circ} + \boldsymbol{a}^{\circ} \times \boldsymbol{b}) \tag{10}$$

$$\| \hat{\boldsymbol{a}} \| = \| \boldsymbol{a} \| + \varepsilon \| \boldsymbol{a}^{\circ} \| \tag{11}$$

$$\operatorname{sgn}(\hat{\boldsymbol{a}}) = \operatorname{sgn}(\boldsymbol{a}) + \varepsilon \operatorname{sgn}(\boldsymbol{a}^{\circ}) \tag{12}$$

$$\lambda(\hat{\boldsymbol{A}}) = \lambda(\boldsymbol{A}) + \varepsilon \lambda(\boldsymbol{A}^{\circ}) \tag{13}$$

where $\hat{\boldsymbol{a}}, \hat{\boldsymbol{b}}$ are dual vectors, $\hat{\boldsymbol{A}}$ is dual matrix, and $\boldsymbol{H}$ is a real matrix, $\lambda(\boldsymbol{A})$ and $\lambda(\boldsymbol{A}^{\circ})$ are the eigenvalues of $\boldsymbol{A}$ and $\boldsymbol{A}^{\circ}$ respectively. Furthermore, in order to simplify the design and deduction in subsequent sections, some special operations are defined:

Inversion

$$\hat{\boldsymbol{A}}^{-1} = \boldsymbol{A}^{-1} - \varepsilon(\boldsymbol{A}^{-1}\boldsymbol{A}^{\circ}\boldsymbol{A}^{-1}), \ \hat{\boldsymbol{A}}\hat{\boldsymbol{A}}^{-1} = \hat{\boldsymbol{A}}^{-1}\hat{\boldsymbol{A}} = \mathbf{I} \tag{14}$$

Respective product

$$\hat{\lambda} \odot \hat{\boldsymbol{a}} = \lambda \boldsymbol{a} + \varepsilon \lambda^{\circ} \boldsymbol{a}^{\circ} \tag{15}$$

$$\hat{\boldsymbol{A}} \odot \hat{\boldsymbol{a}} = \boldsymbol{A}\boldsymbol{a} + \varepsilon \boldsymbol{A}^{\circ}\boldsymbol{a}^{\circ} \tag{16}$$

where $\hat{\lambda}$ is a dual number.

Inner product

$$\left\langle \hat{\boldsymbol{a}}, \hat{\boldsymbol{b}} \right\rangle = \boldsymbol{a}^{\mathrm{T}}\boldsymbol{b} + \boldsymbol{a}^{\circ \mathrm{T}}\boldsymbol{b}^{\circ} \tag{17}$$

B. Dual Quaternions

Dual quaternions are special quaternions in which the scalar part and the vector part are both dual numbers. Hence

$$\hat{\boldsymbol{q}} = \left[\hat{\eta}, \hat{\boldsymbol{\xi}}^{\mathrm{T}} \right]^{\mathrm{T}} = \boldsymbol{q} + \varepsilon \boldsymbol{q}^{\circ} \tag{18}$$

where $\hat{\eta} = \eta + \varepsilon \eta^{\circ}$, $\hat{\boldsymbol{\xi}} = \boldsymbol{\xi} + \varepsilon \boldsymbol{\xi}^{\circ}$ are called the scalar part and vector part of $\hat{\boldsymbol{q}}$ respectively, and $\boldsymbol{q}$, $\boldsymbol{q}^{\circ}$ are called the real part

and dual part of $\hat{\boldsymbol{q}}$ respectively. $\boldsymbol{q}$ is a unit quaternion, which is defined as

$$\boldsymbol{q} \equiv \begin{bmatrix} \eta \\ \boldsymbol{\xi} \end{bmatrix} \equiv \begin{bmatrix} \eta \\ \xi_1 \\ \xi_2 \\ \xi_3 \end{bmatrix} \equiv \eta + \mathrm{i}\xi_1 + \mathrm{j}\xi_2 + \mathrm{k}\xi_3 \tag{19}$$

with

$$\eta^2 + \xi_1^2 + \xi_2^2 + \xi_3^2 = 1 \tag{20}$$

and i, j, k are imaginary units. The conjugate and multiplication of dual quaternions are described by

$$\hat{\boldsymbol{q}}^* = \left[\hat{\eta}, -\hat{\boldsymbol{\xi}}^{\mathrm{T}}\right]^{\mathrm{T}} \tag{21}$$

$$\begin{aligned} \hat{\boldsymbol{q}}_1 \circ \hat{\boldsymbol{q}}_2 &= \boldsymbol{q}_1 \otimes \boldsymbol{q}_2 + \varepsilon(\boldsymbol{q}_1 \otimes \boldsymbol{q}_2^{\circ} + \boldsymbol{q}_1^{\circ} \otimes \boldsymbol{q}_2) \\ &= \left[\hat{\eta}_1\hat{\eta}_2 - \hat{\boldsymbol{\xi}}_1 \cdot \hat{\boldsymbol{\xi}}_2, (\hat{\eta}_1\hat{\boldsymbol{\xi}}_2 + \hat{\eta}_2\hat{\boldsymbol{\xi}}_1 + \hat{\boldsymbol{\xi}}_1 \times \hat{\boldsymbol{\xi}}_2)^{\mathrm{T}}\right]^{\mathrm{T}} \end{aligned} \tag{22}$$

where $\hat{\boldsymbol{q}}_1 = \left[\hat{\eta}_1, \hat{\boldsymbol{\xi}}_1^{\mathrm{T}}\right]^{\mathrm{T}} = \boldsymbol{q}_1 + \varepsilon\boldsymbol{q}_1^{\circ}$ and $\hat{\boldsymbol{q}}_2 = \left[\hat{\eta}_2, \hat{\boldsymbol{\xi}}_2^{\mathrm{T}}\right]^{\mathrm{T}} = \boldsymbol{q}_2 + \varepsilon\boldsymbol{q}_2^{\circ}$, and also here

$$\boldsymbol{q}_1 \otimes \boldsymbol{q}_2 = \left[\eta_1\eta_2 - \boldsymbol{\xi}_1 \cdot \boldsymbol{\xi}_2, (\eta_1\boldsymbol{\xi}_2 + \eta_2\boldsymbol{\xi}_1 + \boldsymbol{\xi}_1 \times \boldsymbol{\xi}_2)^{\mathrm{T}}\right]^{\mathrm{T}} \tag{23}$$

For convenience, define $\hat{\mathbf{1}} = [1,0,0,0] + \varepsilon[1,0,0,0]$ and $\hat{\mathbf{0}} = [0,0,0,0] + \varepsilon[0,0,0,0]$.

Throughout the paper, when a quaternion or a dual quaternion is multiplied with a three-dimensional vector, the three-dimensional vector is regarded as a four-dimensional quaternion or a dual quaternion in which the scalar part is equal to zero, to guarantee that the dimensions are matched.

III. 6-DOF Relative Model of Spacecraft

A target-pursuer spacecraft formation is considered in this paper, and the coordinate frames employed in this paper include: the inertial coordinate frame $\mathcal{F}_I$, the target body coordinate frame $\mathcal{F}_t$, and the pursuer body coordinate frame $\mathcal{F}_p$, as shown in Fig. 1.

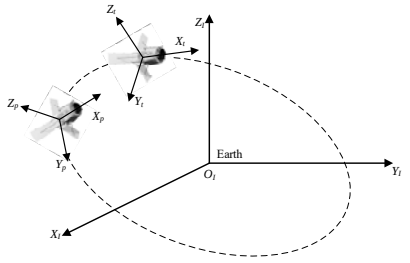

Fig. 1. Coordinate frames

Let $\hat{\boldsymbol{q}}_{pt}$ denote the dual quaternion of $\mathcal{F}_p$ with respect to $\mathcal{F}_t$, and let $\boldsymbol{q}_{pt}$ and $\boldsymbol{p}_{pt}^p$ denote the relative attitude quaternion and relative position between the pursuer and the target respectively. Throughout the paper, $\boldsymbol{a}^*$ represents the variable $\boldsymbol{a}$ expressed in the coordinate frame F_*. Then $\hat{\boldsymbol{q}}_{pt}$ can be written as [12, 13]

$$\hat{\boldsymbol{q}}_{pt} = \boldsymbol{q}_{pt} + \varepsilon\frac{1}{2}\boldsymbol{q}_{pt} \circ \boldsymbol{p}_{pt}^p \tag{24}$$

and the 6-DOF kinematics and dynamics of the pursuer can be described in dual quaternions as [12, 13]

$$2\dot{\hat{\boldsymbol{q}}}_{pt} = \hat{\boldsymbol{q}}_{pt} \circ \hat{\boldsymbol{\omega}}_{pt}^p \tag{25}$$

$$\begin{aligned} &\hat{\boldsymbol{M}}_p\dot{\hat{\boldsymbol{\omega}}}_{pt}^p \\ &= -((\hat{\boldsymbol{\omega}}_{pt}^p + \hat{\boldsymbol{q}}_{pt}^* \circ \hat{\boldsymbol{\omega}}_t^t \circ \hat{\boldsymbol{q}}_{pt}) \times \hat{\boldsymbol{M}}_p(\hat{\boldsymbol{\omega}}_{pt}^p + \hat{\boldsymbol{q}}_{pt}^* \circ \hat{\boldsymbol{\omega}}_t^t \circ \hat{\boldsymbol{q}}_{pt})) \\ &\quad - \hat{\boldsymbol{M}}_p(\hat{\boldsymbol{q}}_{pt}^* \circ \dot{\hat{\boldsymbol{\omega}}}_t^t \circ \hat{\boldsymbol{q}}_{pt}) \\ &\quad + \hat{\boldsymbol{M}}_p(\hat{\boldsymbol{\omega}}_{pt}^p \times (\hat{\boldsymbol{q}}_{pt}^* \circ \hat{\boldsymbol{\omega}}_t^t \circ \hat{\boldsymbol{q}}_{pt})) + \hat{\boldsymbol{F}}_d^p + \hat{\boldsymbol{F}}_u^p + \hat{\boldsymbol{F}}_g^p \end{aligned} \tag{26}$$

where $\hat{\boldsymbol{\omega}}_{pt}^p = \boldsymbol{\omega}_{pt}^p + \varepsilon(\dot{\boldsymbol{p}}_{pt}^p + \boldsymbol{\omega}_{pt}^p \times \boldsymbol{p}_{pt}^p) \in \boldsymbol{R}^3 + \varepsilon\boldsymbol{R}^3$ is the relative dual angular velocity, $\boldsymbol{\omega}_{pt}^p \in \boldsymbol{R}^3$ is the relative angular velocity of the pursuer with respect to the target, and $\hat{\boldsymbol{\omega}}_t^t$ is the dual angular velocity of the target, $\hat{\boldsymbol{F}}_u^p = \boldsymbol{f}_u^p + \varepsilon\boldsymbol{\tau}_u^p \in \boldsymbol{R}^3 + \varepsilon\boldsymbol{R}^3$ is the dual control input, $\boldsymbol{f}_u^p$ and $\boldsymbol{\tau}_u^p$ are the control force and the control torque respectively, $\hat{\boldsymbol{F}}_d^p$ is the external disturbance input, and $\hat{\boldsymbol{F}}_g^p = \boldsymbol{f}_g^p + \varepsilon\boldsymbol{\tau}_g^p \in \boldsymbol{R}^3 + \varepsilon\boldsymbol{R}^3$ is the gravitational input. The gravitational force and the gravity gradient torque are $\boldsymbol{f}_g^p = -\left(\mu m_p / r_p^3\right)\boldsymbol{r}_p$ and $\boldsymbol{\tau}_g^p$, respectively, where μ is the gravitational constant and $\boldsymbol{r}_p$ is the position vector of the pursuer with respect to the mass center of the Earth. The matrix $\hat{\boldsymbol{M}}_p = m_p\frac{\mathrm{d}}{\mathrm{d}\varepsilon}\mathbf{I} + \varepsilon\boldsymbol{J}_p$ is called the dual mass, where m_p and $\boldsymbol{J}_p$ are the mass and the inertia of the pursuer respectively.

Rewriting the relative dual quaternion as a combination of the scalar part and the vector part, $\hat{\boldsymbol{q}}_{pt} = \left[\hat{\eta}_{pt}, \hat{\boldsymbol{\xi}}_{pt}^{\mathrm{T}}\right]^{\mathrm{T}}$, and substituting into Eq. (25), gives

$$\begin{cases} \dot{\hat{\eta}}_{pt} = -\frac{1}{2}\hat{\boldsymbol{\xi}}_{pt}^{\mathrm{T}}\hat{\boldsymbol{\omega}}_{pt}^p \\ \dot{\hat{\boldsymbol{\xi}}}_{pt} = \frac{1}{2}(\hat{\boldsymbol{\xi}}_{pt}^{\times} + \hat{\eta}_{pt}\mathbf{I})\hat{\boldsymbol{\omega}}_{pt}^p \end{cases} \tag{27}$$

where $\hat{\boldsymbol{\xi}}_{pt}^{\times} = \boldsymbol{\xi}_{pt}^{\times} + \varepsilon\boldsymbol{\xi}_{pt}^{\circ\times}$, and here $\boldsymbol{a}^{\times}$ denotes the skew-symmetric matrix of vector $\boldsymbol{a} = [a_x \quad a_y \quad a_z]^{\mathrm{T}}$:

$$\boldsymbol{a}^{\times}=\begin{bmatrix}0 & -a_z & a_y\\ a_z & 0 & -a_x\\ -a_y & a_x & 0\end{bmatrix} \tag{28}$$

Define $\hat{\boldsymbol{Z}}=\boldsymbol{Z}+\varepsilon\boldsymbol{Z}^{\circ}=0.5(\hat{\boldsymbol{\xi}}_{pt}^{\times}+\hat{\eta}_{pt}\mathbf{I})$, $\hat{\boldsymbol{Q}}=\left[0.5(\hat{\boldsymbol{\xi}}_{pt}^{\times}+\hat{\eta}_{pt}\mathbf{I})\right]^{-1}$, so that $\hat{\boldsymbol{Q}}\dot{\hat{\boldsymbol{\xi}}}_{pt}=\hat{\boldsymbol{\omega}}_{pt}^{p}$ and $\dot{\hat{\boldsymbol{Q}}}\dot{\hat{\boldsymbol{\xi}}}_{pt}+\hat{\boldsymbol{Q}}\ddot{\hat{\boldsymbol{\xi}}}_{pt}=\dot{\hat{\boldsymbol{\omega}}}_{pt}^{p}$. Substituting these equations into Eq. (27), a Lagrange-like dynamics based on dual quaternion is obtained as

$$\hat{\boldsymbol{M}}_p(\hat{\boldsymbol{Q}}\ddot{\hat{\boldsymbol{\xi}}}_{pt})+\hat{\boldsymbol{B}}(\hat{\boldsymbol{Q}}\dot{\hat{\boldsymbol{\xi}}}_{pt})+\hat{\boldsymbol{G}}=\hat{\boldsymbol{F}}_u^{p}+\hat{\boldsymbol{F}}_d^{p}+\hat{\boldsymbol{F}}_g^{p} \tag{29}$$

where

$$\begin{aligned}\hat{\boldsymbol{G}}=&(\hat{\boldsymbol{Q}}\dot{\hat{\boldsymbol{\xi}}}_{pt}+\hat{\boldsymbol{q}}_{pt}^{*}\circ\hat{\boldsymbol{\omega}}_t^{t}\circ\hat{\boldsymbol{q}}_{pt})^{\times}(\hat{\boldsymbol{M}}_p(\hat{\boldsymbol{q}}_{pt}^{*}\circ\hat{\boldsymbol{\omega}}_t^{t}\circ\hat{\boldsymbol{q}}_{pt}))\\&+\hat{\boldsymbol{M}}_p(\hat{\boldsymbol{Q}}\dot{\hat{\boldsymbol{\xi}}}_{pt})+\hat{\boldsymbol{M}}_p(\hat{\boldsymbol{q}}_{pt}^{*}\circ\dot{\hat{\boldsymbol{\omega}}}_t^{t}\circ\hat{\boldsymbol{q}}_{pt})\\&-\hat{\boldsymbol{M}}_p((\hat{\boldsymbol{Q}}\dot{\hat{\boldsymbol{\xi}}}_{pt})^{\times}(\hat{\boldsymbol{q}}_{pt}^{*}\circ\hat{\boldsymbol{\omega}}_t^{t}\circ\hat{\boldsymbol{q}}_{pt}))\end{aligned}$$

and $\hat{\boldsymbol{B}}=(\hat{\boldsymbol{Q}}\dot{\hat{\boldsymbol{\xi}}}_{pt}+\hat{\boldsymbol{q}}_{pt}^{*}\circ\hat{\boldsymbol{\omega}}_t^{t}\circ\hat{\boldsymbol{q}}_{pt})^{\times}\hat{\boldsymbol{M}}_p$.

The actuators of the pursuer spacecraft are assumed to be faulty, and the fault types considered in this paper include [23]:

a) **Partial energy loss**: actuator can only output part of the expected force or torque;
b) **Complete energy loss**: actuator cannot output any force or torque;
c) **Zero and continuous float**: actuator can't output the expected force or torque accurately, and a small DC offset exists.
d) **Locking**: actuator has a fixed and uncontrolled output.

One expression for the control input that can describe all categories of the faults mentioned above is

$$\hat{\boldsymbol{F}}_u^{p}=\hat{\boldsymbol{A}}\odot\hat{\boldsymbol{F}}_{uo}^{p}=\hat{\boldsymbol{A}}\odot[\hat{\boldsymbol{H}}(t)\odot\hat{\boldsymbol{F}}_{uc}+\hat{\boldsymbol{F}}_f] \tag{30}$$

where $\hat{\boldsymbol{A}}=\boldsymbol{A}+\varepsilon\boldsymbol{A}^{\circ}$ is called the control allocation matrix, $\boldsymbol{A}\in\mathbb{R}^{3\times n}$ and $\boldsymbol{A}^{\circ}\in\mathbb{R}^{3\times l}$, and n and l are the numbers of the force actuators and torque actuators respectively. $\hat{\boldsymbol{H}}(t)=\boldsymbol{H}(t)+\varepsilon\boldsymbol{H}^{\circ}(t)$ is called fault matrix, and here we assume $\boldsymbol{H}=\mathrm{diag}(h_1,h_2,..,h_n)$, $\boldsymbol{H}^{\circ}=\mathrm{diag}(h_1^{\circ},h_2^{\circ},..,h_l^{\circ})$, where $h_i,h_j^{\circ}\in[0,1],\ i=1,2,..,n,\ j=1,2,..,l$. $\hat{\boldsymbol{H}}(t)$ is used to describe faults *a* and *b*. $\hat{\boldsymbol{F}}_{uc}=\boldsymbol{F}_{uc}+\varepsilon\boldsymbol{\tau}_{uc}$ is the expected control input of the actuators, while $\boldsymbol{F}_{uc}\in\mathbb{R}^{n}$ and $\boldsymbol{\tau}_{uc}\in\mathbb{R}^{l}$ are the expected control force and control torque respectively. $\hat{\boldsymbol{F}}_f=\boldsymbol{F}_f+\varepsilon\boldsymbol{\tau}_f$ is the float or locking value of the actuators. Notice that for matrices/vectors $\hat{\boldsymbol{A}}$, $\hat{\boldsymbol{H}}$ and $\hat{\boldsymbol{F}}_{uc}$, the dimensions of their dual parts are different to the dimensions of their real parts; these matrices/vectors are a kind of "special dual matrix/vector", and only a few operations defined previously, such as "$\pm$" and "$\odot$", can be applied to them.

Then substituting Eq. (30) into Eq. (29), the 6-DOF relative dynamics of the pursuer spacecraft used in this paper is obtained as

$$\begin{aligned}\hat{\boldsymbol{M}}_p(\hat{\boldsymbol{Q}}\ddot{\hat{\boldsymbol{\xi}}}_{pt})+\hat{\boldsymbol{B}}(\hat{\boldsymbol{Q}}\dot{\hat{\boldsymbol{\xi}}}_{pt})+\hat{\boldsymbol{G}}=&\hat{\boldsymbol{A}}\odot[\hat{\boldsymbol{H}}(t)\odot\hat{\boldsymbol{F}}_{uc}+\hat{\boldsymbol{F}}_f]\\&+\hat{\boldsymbol{F}}_d^{p}+\hat{\boldsymbol{F}}_g^{p}\end{aligned} \tag{31}$$

Based on the 6-DOF dynamics given by Eq. (31) and the assumptions above, the control objective of this paper can be given as: design a control law $\hat{\boldsymbol{F}}_{uc}$, so that the tracking error $\hat{\boldsymbol{\xi}}_{pt}$ converges to zero within a finite time t_f, formulated as

$$\forall t\geq t_f,\ \hat{\boldsymbol{\xi}}_{pt}(t)\equiv\mathbf{0}+\varepsilon\mathbf{0} \tag{32}$$

Remark 1: The Lagrange-like model described in Eq. (31) is a 6-DOF coupled model. It can be embodied by $\hat{\boldsymbol{q}}_{pt}=\boldsymbol{q}_{pt}+\varepsilon 0.5\boldsymbol{q}_{pt}\circ\boldsymbol{p}_{pt}^{p}$ and $\hat{\boldsymbol{\omega}}_{pt}^{p}=\boldsymbol{\omega}_{pt}^{p}+\varepsilon(\dot{\boldsymbol{p}}_{pt}^{p}+\boldsymbol{\omega}_{pt}^{p}\times\boldsymbol{p}_{pt}^{p})$, which shows that relative position motion contains attitude information.

IV. Control Law Design and Stability Analysis

In this section, a novel adaptive fault-tolerant controller is proposed, and the finite-time convergence of the closed-loop system is discussed.

Before proposing the control law, some reasonable assumptions and deductions are made. The mass and inertia of the pursuer is likely to be uncertain, but must be bounded within certain ranges. Hence there exists dual numbers $\hat{b}_1=b_1\frac{\mathrm{d}}{\mathrm{d}\varepsilon}+\varepsilon b_1^{\circ}$, with $b_1>\|m_p\|, b_1^{\circ}>\|\boldsymbol{J}_p\|$, and $\hat{b}_2=b_2\frac{\mathrm{d}}{\mathrm{d}\varepsilon}+\varepsilon b_2^{\circ}$, with $b_2>\|\boldsymbol{J}_p^{-1}\|, b_2^{\circ}>\|m^{-1}\|$, which are known and satisfy the following two inequalities: $\|\hat{\boldsymbol{M}}_p\|=\|m_p\frac{\mathrm{d}}{\mathrm{d}\varepsilon}\mathbf{I}+\varepsilon\boldsymbol{J}_p\|=\|m_p\|\frac{\mathrm{d}}{\mathrm{d}\varepsilon}+\varepsilon\|\boldsymbol{J}_p\|\leq\hat{b}_1$ and $\|\hat{\boldsymbol{M}}_p^{-1}\|=\|\boldsymbol{J}_p^{-1}\frac{\mathrm{d}}{\mathrm{d}\varepsilon}+\varepsilon m^{-1}\mathbf{I}\|=\|\boldsymbol{J}_p^{-1}\|\frac{\mathrm{d}}{\mathrm{d}\varepsilon}+\varepsilon\|m^{-1}\|\leq\hat{b}_2$. The derivative of the expected dual angular velocity satisfies $\|\dot{\hat{\boldsymbol{\omega}}}_t^{t}\|\leq\hat{b}_3=b_3+\varepsilon b_3^{\circ}$, with $b_3,b_3^{\circ}>0$. The float errors of the actuators and the external disturbances are also bounded, so that $\|\hat{\boldsymbol{F}}_f\|\leq\hat{b}_4=b_4+\varepsilon b_4^{\circ}$, with $b_4,b_4^{\circ}>0$, and $\|\hat{\boldsymbol{F}}_d^{p}+\hat{\boldsymbol{F}}_g^{p}\|\leq\hat{b}_5=b_5+\varepsilon b_5^{\circ}$, with $b_5,b_5^{\circ}>0$. Based on these assumptions, we review the formulas of $\hat{\boldsymbol{B}}$ and $\hat{\boldsymbol{G}}$, and since $\hat{\boldsymbol{Q}}\dot{\hat{\boldsymbol{\xi}}}_{pt}=\hat{\boldsymbol{\omega}}_{pt}^{p}$, one can obtain:

$$\| \hat{\boldsymbol{B}} \| = \| (\hat{\boldsymbol{Q}}\dot{\hat{\boldsymbol{\xi}}}_{pt} + \hat{\boldsymbol{q}}^{*}_{pt} \circ \hat{\boldsymbol{\omega}}^{t}_{t} \circ \hat{\boldsymbol{q}}_{pt})^{\times} \hat{\boldsymbol{M}}_{p} \| \leq (\| \hat{\boldsymbol{\omega}}^{p}_{pt} \| + \| \hat{\boldsymbol{\omega}}^{t}_{t} \|) \hat{b}_1 \quad (33)$$

$$\begin{aligned} \| \hat{\boldsymbol{G}} \| &= \| (\hat{\boldsymbol{Q}}\dot{\hat{\boldsymbol{\xi}}}_{pt} + \hat{\boldsymbol{q}}^{*}_{pt} \circ \hat{\boldsymbol{\omega}}^{t}_{t} \circ \hat{\boldsymbol{q}}_{pt})^{\times} (\hat{\boldsymbol{M}}_{p} (\hat{\boldsymbol{q}}^{*}_{pt} \circ \hat{\boldsymbol{\omega}}^{t}_{t} \circ \hat{\boldsymbol{q}}_{pt})) \\ &+ \hat{\boldsymbol{M}}_{p} (\dot{\hat{\boldsymbol{Q}}}\dot{\hat{\boldsymbol{\xi}}}_{pt}) + \hat{\boldsymbol{M}}_{p} (\hat{\boldsymbol{q}}^{*}_{pt} \circ \dot{\hat{\boldsymbol{\omega}}}^{t}_{t} \circ \hat{\boldsymbol{q}}_{pt}) \\ &- \hat{\boldsymbol{M}}_{p} ((\hat{\boldsymbol{Q}}\dot{\hat{\boldsymbol{\xi}}}_{pt})^{\times} (\hat{\boldsymbol{q}}^{*}_{pt} \circ \hat{\boldsymbol{\omega}}^{t}_{t} \circ \hat{\boldsymbol{q}}_{pt})) \| \\ &\leq (\| \hat{\boldsymbol{\omega}}^{p}_{pt} \| + \| \hat{\boldsymbol{\omega}}^{t}_{t} \|) (\hat{b}_1 \| \hat{\boldsymbol{\omega}}^{t}_{t} \|) \\ &+ \| \hat{\boldsymbol{M}}_{p} \| \| \hat{\boldsymbol{Q}}\dot{\hat{\boldsymbol{\xi}}}_{pt} \| + \| \hat{\boldsymbol{M}}_{p} \| \hat{b}_3 + \| \hat{\boldsymbol{M}}_{p} \| (\| \hat{\boldsymbol{\omega}}^{t}_{t} \| \| \hat{\boldsymbol{\omega}}^{p}_{pt} \|) \end{aligned} \quad (34)$$

Then according to Eqs. (33) and (34), one can further obtain

$$\begin{aligned} &\| \hat{\boldsymbol{Z}} \hat{\boldsymbol{M}}^{-1}_{p} (-\hat{\boldsymbol{B}} (\hat{\boldsymbol{Q}}\dot{\hat{\boldsymbol{\xi}}}_{pt}) - \hat{\boldsymbol{G}} + \hat{\boldsymbol{A}} \odot \hat{\boldsymbol{F}}_{f} + \hat{\boldsymbol{F}}^{p}_{d} + \hat{\boldsymbol{F}}^{p}_{g}) + k\dot{\hat{\boldsymbol{\xi}}}_{pt} - \dot{\hat{\boldsymbol{f}}}(t) \| \\ &\leq \| \hat{\boldsymbol{Z}} \| \hat{b}_2 ((\| \hat{\boldsymbol{\omega}}^{p}_{pt} \| + \| \hat{\boldsymbol{\omega}}^{t}_{t} \|) \hat{b}_1 \| \hat{\boldsymbol{\omega}}^{p}_{pt} \|) \\ &\quad + \| \hat{\boldsymbol{Z}} \| \hat{b}_2 ((\| \hat{\boldsymbol{\omega}}^{p}_{pt} \| + \| \hat{\boldsymbol{\omega}}^{t}_{t} \|) (\hat{b}_1 \| \hat{\boldsymbol{\omega}}^{t}_{t} \|)) + \| \hat{\boldsymbol{Z}} \| \| \hat{\boldsymbol{Q}}\dot{\hat{\boldsymbol{\xi}}}_{pt} \| \\ &\quad + \| \hat{\boldsymbol{Z}} \| \hat{b}_3 + \| \hat{\boldsymbol{Z}} \| (\| \hat{\boldsymbol{\omega}}^{t}_{t} \| \| \hat{\boldsymbol{\omega}}^{p}_{pt} \|) \\ &\quad + \| \hat{\boldsymbol{Z}} \| \hat{b}_2 (\hat{b}_4 \| \hat{\boldsymbol{A}} \| + \hat{b}_5) + k \| \dot{\hat{\boldsymbol{\xi}}}_{pt} \| + \| \dot{\hat{\boldsymbol{f}}}(t) \| \\ &= \| \hat{\boldsymbol{Z}} \| \hat{b}_2 (\| \hat{\boldsymbol{\omega}}^{p}_{pt} \| (\hat{b}_1 \| \hat{\boldsymbol{\omega}}^{p}_{pt} \|)) + \| \hat{\boldsymbol{Z}} \| \hat{b}_2 ((\| \hat{\boldsymbol{\omega}}^{t}_{t} \|) (\hat{b}_1 \| \hat{\boldsymbol{\omega}}^{p}_{pt} \|) \\ &\quad + (\hat{b}_1 \| \hat{\boldsymbol{\omega}}^{t}_{t} \|) \| \hat{\boldsymbol{\omega}}^{p}_{pt} \|) + \| \hat{\boldsymbol{Z}} \| (\| \hat{\boldsymbol{\omega}}^{t}_{t} \| \| \hat{\boldsymbol{\omega}}^{p}_{pt} \|) \\ &\quad + \| \hat{\boldsymbol{Z}} \| \hat{b}_2 (\hat{b}_4 \| \hat{\boldsymbol{A}} \|) + k \| \dot{\hat{\boldsymbol{\xi}}}_{pt} \| + \| \dot{\hat{\boldsymbol{f}}}(t) \| + \| \hat{\boldsymbol{Z}} \| \| \hat{\boldsymbol{Q}}\dot{\hat{\boldsymbol{\xi}}}_{pt} \| \\ &\quad + \| \hat{\boldsymbol{Z}} \| \hat{b}_2 ((\hat{b}_1 \| \hat{\boldsymbol{\omega}}^{t}_{t} \|) \| \hat{\boldsymbol{\omega}}^{t}_{t} \|) + \| \hat{\boldsymbol{Z}} \| \hat{b}_3 + \| \hat{\boldsymbol{Z}} \| \hat{b}_2 \hat{b}_5 \\ &= \hat{\nu} + \| \hat{\boldsymbol{Z}} \| \hat{\varsigma} \end{aligned} \quad (35)$$

where $\hat{\varsigma} = \hat{b}_2 (\hat{b}_4 \| \hat{\boldsymbol{A}} \|) + \hat{b}_3 + \hat{b}_2 \hat{b}_5$, and

$$\begin{aligned} \hat{\nu} &= \| \hat{\boldsymbol{Z}} \| \hat{b}_2 (\| \hat{\boldsymbol{\omega}}^{p}_{pt} \| (\hat{b}_1 \| \hat{\boldsymbol{\omega}}^{p}_{pt} \|)) + \| \hat{\boldsymbol{Z}} \| \hat{b}_2 ((\| \hat{\boldsymbol{\omega}}^{t}_{t} \|) (\hat{b}_1 \| \hat{\boldsymbol{\omega}}^{p}_{pt} \|) \\ &\quad + (\hat{b}_1 \| \hat{\boldsymbol{\omega}}^{t}_{t} \|) \| \hat{\boldsymbol{\omega}}^{p}_{pt} \|) + \| \hat{\boldsymbol{Z}} \| (\| \hat{\boldsymbol{\omega}}^{t}_{t} \| \| \hat{\boldsymbol{\omega}}^{p}_{pt} \|) \\ &\quad + k \| \dot{\hat{\boldsymbol{\xi}}}_{pt} \| + \| \dot{\hat{\boldsymbol{f}}}(t) \| + \| \hat{\boldsymbol{Z}} \| \| \hat{\boldsymbol{Q}}\dot{\hat{\boldsymbol{\xi}}}_{pt} \| + \| \hat{\boldsymbol{Z}} \| \hat{b}_2 ((\hat{b}_1 \| \hat{\boldsymbol{\omega}}^{t}_{t} \|) \| \hat{\boldsymbol{\omega}}^{t}_{t} \|) \end{aligned}$$

For convenience, the form of $\| \hat{\boldsymbol{Z}} \| \hat{\varsigma}$ is changed to $\| \hat{\boldsymbol{Z}} \| \hat{\varsigma} = \hat{\boldsymbol{\eta}}^{\mathrm{T}} \odot \hat{\boldsymbol{\gamma}}$, where $\hat{\boldsymbol{\eta}} = [\varsigma + \varepsilon\varsigma \quad 0 + \varepsilon\varsigma^{\circ}]^{\mathrm{T}}$ and $\hat{\boldsymbol{\gamma}} = [\| \boldsymbol{Z} \| + \varepsilon \| \boldsymbol{Z}^{\circ} \| \quad 0 + \varepsilon \| \boldsymbol{Z} \|]^{\mathrm{T}}$, so that

$$\begin{aligned} &\| \hat{\boldsymbol{Z}} \hat{\boldsymbol{M}}^{-1}_{p} (-\hat{\boldsymbol{B}} (\hat{\boldsymbol{Q}}\dot{\hat{\boldsymbol{\xi}}}_{pt}) - \hat{\boldsymbol{G}} + \hat{\boldsymbol{A}} \odot \hat{\boldsymbol{F}}_{f} + \hat{\boldsymbol{F}}^{p}_{d}) + k\dot{\hat{\boldsymbol{\xi}}}_{pt} - \dot{\hat{\boldsymbol{f}}}(t) \| \\ &\leq \hat{\nu} + \hat{\boldsymbol{\eta}}^{\mathrm{T}} \odot \hat{\boldsymbol{\gamma}} \end{aligned} \quad (36)$$

Note that $\hat{\nu}$ and $\hat{\boldsymbol{\gamma}}$ can be estimated while $\hat{\boldsymbol{\eta}}$ is unknown for the controller.

The main result of the paper is summarized as follows.

Theorem 1: Considering the 6-DOF target-pursuer spacecraft control system given in Eq. (31), and employing the novel time-varying sliding manifold:

$$\hat{\boldsymbol{s}} = \dot{\hat{\boldsymbol{\xi}}}_{pt} + k\hat{\boldsymbol{\xi}}_{pt} - \hat{\boldsymbol{f}}(t) \quad (37)$$

$$\hat{\boldsymbol{f}}(t) = \begin{cases} \dot{\hat{\boldsymbol{\xi}}}_{pt}(0) + k\hat{\boldsymbol{\xi}}_{pt}(0) & 0 \leq t < t_m \\ (1 - \tau(t - t_m))(\dot{\hat{\boldsymbol{\xi}}}_{pt}(0) & \\ + k\hat{\boldsymbol{\xi}}_{pt}(0)) \cos(\dfrac{\pi(t - t_m)}{2(t_f - t_m)}) & \text{if } t_m \leq t < t_f \\ \hat{\boldsymbol{0}} & \text{if } t \geq t_f \end{cases} \quad (38)$$

where $k>0$ is a constant, $\dot{\hat{\boldsymbol{\xi}}}_{pt}(0)$ and $\hat{\boldsymbol{\xi}}_{pt}(0)$ are the initial values of $\dot{\hat{\boldsymbol{\xi}}}_{pt}$ and $\hat{\boldsymbol{\xi}}_{pt}$ respectively, t_m and t_f are finite times with $0<t_m< t_f$, and τ is a constant dual matrix to be designed. The control law and adaptive laws are defined as

$$\begin{aligned} \hat{\boldsymbol{F}}_{uc} = &-\hat{\boldsymbol{A}}^{\mathrm{T}} \odot (\hat{b}_1 (\hat{\boldsymbol{Q}} ((\hat{h} \odot \hat{\nu} + \hat{\boldsymbol{\chi}}^{\mathrm{T}} \odot \hat{\boldsymbol{\gamma}}) \odot \operatorname{sgn}(\hat{\boldsymbol{s}})))) \\ &- \hat{\boldsymbol{A}}^{\mathrm{T}} \odot (\hat{b}_1 (\hat{\boldsymbol{Q}} (\hat{k}_c \odot \operatorname{sgn}(\hat{\boldsymbol{s}})))) \end{aligned} \quad (39)$$

$$\dot{\hat{\boldsymbol{\chi}}} = -\alpha_1^{\,2} \hat{\boldsymbol{\chi}} + \kappa_1 \langle \hat{\boldsymbol{s}}, \operatorname{sgn}(\hat{\boldsymbol{s}}) \rangle \hat{\boldsymbol{\gamma}}, \ \hat{\boldsymbol{\chi}}(0) > \hat{\boldsymbol{0}} \quad (40)$$

$$\dot{\hat{h}} = -\alpha_2^{\,2} \hat{h} + \kappa_2 \langle \hat{\boldsymbol{s}}, \operatorname{sgn}(\hat{\boldsymbol{s}}) \rangle \hat{\nu}, \hat{h}(0) > \hat{0} \quad (41)$$

where $\hat{k}_c > \hat{0}$ is a constant dual number, $\alpha_1, \alpha_2, \kappa_1, \kappa_2 > 0$ are constant real numbers, and $\hat{\boldsymbol{\chi}}$ is the estimated value of $\hat{\boldsymbol{\eta}}$. If $\lambda = \min(\lambda_1, \lambda_1^{\circ})$, where $\hat{\lambda}_1 = \lambda_1 + \varepsilon\lambda_1^{\circ} = \lambda_{\min} (\hat{\boldsymbol{A}} \odot \hat{\boldsymbol{H}}(t) \odot \hat{\boldsymbol{A}}^{\mathrm{T}})$, satisfies $\lambda > 0$, then by choosing an appropriate τ, the closed-loop system is guaranteed to be finite-time stable, and satisfies $\hat{\boldsymbol{\xi}}_{pt} \equiv \boldsymbol{0}, \ \forall t \geq t_f$.

Proof: The proof is divided into two steps. First, it is proved that the sliding condition holds after $t \geq t_m$, and second, it is proved that the tracking error $\hat{\boldsymbol{\xi}}_{pt}$ converges to zero within the finite time t_f.

Step 1: Define a candidate Lyapunov function as

$$\begin{aligned} V = &\frac{1}{2} \langle \hat{\boldsymbol{s}}, \hat{\boldsymbol{s}} \rangle + \frac{1}{2\kappa_1 \lambda} \langle \hat{\boldsymbol{\eta}} - \lambda \hat{\boldsymbol{\chi}}, \hat{\boldsymbol{\eta}} - \lambda \hat{\boldsymbol{\chi}} \rangle \\ &+ \frac{1}{2\kappa_2 \lambda} \langle \hat{1} - \lambda \hat{h}, \hat{1} - \lambda \hat{h} \rangle \end{aligned} \quad (42)$$

The derivative of V with respect to t is:

$$\begin{aligned}\dot{V} &= \left\langle \hat{\boldsymbol{s}}, \hat{\boldsymbol{Q}}^{-1}\hat{\boldsymbol{M}}_p^{-1}(\hat{\boldsymbol{M}}_p(\ddot{\hat{\boldsymbol{Q}}}\ddot{\hat{\boldsymbol{\xi}}}_{pt})) + k\ddot{\hat{\boldsymbol{\xi}}}_{pt} - \dot{\hat{\boldsymbol{f}}}(t)\right\rangle \\ &\quad - \frac{\left\langle \hat{\boldsymbol{\eta}} - \lambda\hat{\boldsymbol{\chi}}, \dot{\hat{\boldsymbol{\chi}}}\right\rangle}{\kappa_1} - \frac{1}{\kappa_2}\left\langle \hat{1} - \lambda\hat{h}, \dot{\hat{h}}\right\rangle \\ &= \left\langle \begin{array}{l} \hat{\boldsymbol{s}}, \hat{\boldsymbol{Q}}^{-1}\hat{\boldsymbol{M}}_p^{-1}\left(\begin{array}{l} -\hat{\boldsymbol{B}}(\hat{\boldsymbol{Q}}\ddot{\hat{\boldsymbol{\xi}}}_{pt}) - \hat{\boldsymbol{G}} + \\ \hat{\boldsymbol{A}} \odot [\hat{\boldsymbol{H}}(t) \odot \hat{\boldsymbol{F}}_{uc} + \hat{\boldsymbol{F}}_f] + \hat{\boldsymbol{F}}_d^p \end{array}\right) \\ +k\ddot{\hat{\boldsymbol{\xi}}}_{pt} - \dot{\hat{\boldsymbol{f}}}(t) \end{array}\right\rangle \\ &\quad - \frac{\left\langle \hat{\boldsymbol{\eta}} - \lambda\hat{\boldsymbol{\chi}}, \dot{\hat{\boldsymbol{\chi}}}\right\rangle}{\kappa_1} - \frac{1}{\kappa_2}\left\langle \hat{1} - \lambda\hat{h}, \dot{\hat{h}}\right\rangle \\ &\le \left\langle \begin{array}{l} \hat{\boldsymbol{s}}, \hat{\boldsymbol{Q}}^{-1}\hat{\boldsymbol{M}}_p^{-1}(\hat{\boldsymbol{A}} \odot \hat{\boldsymbol{H}}(t) \odot \hat{\boldsymbol{F}}_{uc}) \\ +(\hat{\nu} + \hat{\boldsymbol{\eta}}^{\mathrm{T}} \odot \hat{\boldsymbol{\gamma}}) \odot \mathrm{sgn}(\hat{\boldsymbol{s}}) \end{array}\right\rangle \\ &\quad - \frac{\left\langle \hat{\boldsymbol{\eta}} - \lambda\hat{\boldsymbol{\chi}}, \dot{\hat{\boldsymbol{\chi}}}\right\rangle}{\kappa_1} - \frac{1}{\kappa_2}\left\langle \hat{1} - \lambda\hat{h}, \dot{\hat{h}}\right\rangle \end{aligned} \tag{43}$$

Substituting control law Eq. (39) into Eq. (43) yields

$$\begin{aligned}\dot{V} &\le \left\langle \begin{array}{l} \hat{\boldsymbol{s}}, \hat{\boldsymbol{Q}}^{-1}\hat{\boldsymbol{M}}_p^{-1}(\hat{\boldsymbol{A}} \odot \hat{\boldsymbol{H}}(t) \odot \\ (-\hat{\boldsymbol{A}}^{\mathrm{T}} \odot (\hat{b}_1(\hat{\boldsymbol{Q}}((\hat{h} \odot \hat{\nu} + \hat{\boldsymbol{\chi}}^{\mathrm{T}} \odot \hat{\boldsymbol{\gamma}}) \odot \mathrm{sgn}(\hat{\boldsymbol{s}}))))) \\ -\hat{\boldsymbol{A}}^{\mathrm{T}} \odot (\hat{b}_1(\hat{\boldsymbol{Q}}(\hat{k}_c \odot \mathrm{sgn}(\hat{\boldsymbol{s}}))))) \\ +(\hat{\nu} + \hat{\boldsymbol{\eta}}^{\mathrm{T}} \odot \hat{\boldsymbol{\gamma}}) \odot \mathrm{sgn}(\hat{\boldsymbol{s}}) \end{array}\right\rangle \\ &\quad - \frac{\left\langle \hat{\boldsymbol{\eta}} - \lambda\hat{\boldsymbol{\chi}}, \dot{\hat{\boldsymbol{\chi}}}\right\rangle}{\kappa_1} - \frac{1}{\kappa_2}\left\langle \hat{1} - \lambda\hat{h}, \dot{\hat{h}}\right\rangle \\ &\le -\left\langle \begin{array}{l} \hat{\boldsymbol{s}}, ((\lambda\hat{h} - \hat{1}) \odot \hat{\nu}) \odot \mathrm{sgn}(\hat{\boldsymbol{s}}) \\ +(\lambda\hat{\boldsymbol{\chi}} - \hat{\boldsymbol{\eta}}) \odot \hat{\boldsymbol{\gamma}} \odot \mathrm{sgn}(\hat{\boldsymbol{s}}) + \lambda\hat{k}_c \odot \mathrm{sgn}(\hat{\boldsymbol{s}}) \end{array}\right\rangle \\ &\quad - \frac{\left\langle \hat{\boldsymbol{\eta}} - \lambda\hat{\boldsymbol{\chi}}, \dot{\hat{\boldsymbol{\chi}}}\right\rangle}{\kappa_1} - \frac{1}{\kappa_2}\left\langle \hat{1} - \lambda\hat{h}, \dot{\hat{h}}\right\rangle \end{aligned} \tag{44}$$

Then substituting adaptive laws Eq. (40) and Eq. (41) into Eq.(44), gives

$$\begin{aligned}\dot{V} &\le -\left\langle \begin{array}{l} \hat{\boldsymbol{s}}, ((\lambda\hat{h} - \hat{1}) \odot \hat{\nu}) \odot \mathrm{sgn}(\hat{\boldsymbol{s}}) \\ +(\lambda\hat{\boldsymbol{\chi}} - \hat{\boldsymbol{\eta}}) \odot \hat{\boldsymbol{\gamma}} \odot \mathrm{sgn}(\hat{\boldsymbol{s}}) + \lambda\hat{k}_c \odot \mathrm{sgn}(\hat{\boldsymbol{s}}) \end{array}\right\rangle \\ &\quad - \frac{\left\langle \hat{\boldsymbol{\eta}} - \lambda\hat{\boldsymbol{\chi}}, -\alpha_1^{\,2}\hat{\boldsymbol{\chi}} + \kappa_1\left\langle \hat{\boldsymbol{s}}, \mathrm{sgn}(\hat{\boldsymbol{s}})\right\rangle\hat{\boldsymbol{\gamma}}\right\rangle}{\kappa_1} \\ &\quad - \frac{1}{\kappa_2}\left\langle \hat{1} - \lambda\hat{h}, -\alpha_2^{\,2}\hat{h} + \kappa_2\left\langle \hat{\boldsymbol{s}}, \mathrm{sgn}(\hat{\boldsymbol{s}})\right\rangle\hat{\nu}\right\rangle \\ &\le -\left\langle \hat{\boldsymbol{s}}, \lambda\hat{k}_c \odot \mathrm{sgn}(\hat{\boldsymbol{s}})\right\rangle + \frac{\left\langle \hat{\boldsymbol{\eta}} - \lambda\hat{\boldsymbol{\chi}}, \alpha_1^{\,2}\hat{\boldsymbol{\chi}}\right\rangle}{\kappa_1} + \frac{\left\langle \hat{1} - \lambda\hat{h}, \alpha_2^{\,2}\hat{h}\right\rangle}{\kappa_2} \end{aligned} \tag{45}$$

According to the properties of the sum of squares, for any constant number l>0.5

$$\begin{aligned} &\frac{\left\langle \hat{\boldsymbol{\eta}} - \lambda\hat{\boldsymbol{\chi}}, \alpha_1^{\,2}\hat{\boldsymbol{\chi}}\right\rangle}{\kappa_1} + \frac{\left\langle \hat{1} - \lambda\hat{h}, \alpha_2^{\,2}\hat{h}\right\rangle}{\kappa_2} \\ &= -\frac{\alpha_1^{\,2}}{\lambda\kappa_1}\left\langle \hat{\boldsymbol{\eta}} - \lambda\hat{\boldsymbol{\chi}}, \hat{\boldsymbol{\eta}} - \lambda\hat{\boldsymbol{\chi}} - \hat{\boldsymbol{\eta}}\right\rangle - \frac{\alpha_2^{\,2}}{\lambda\kappa_2}\left\langle \hat{1} - \lambda\hat{h}, \hat{1} - \lambda\hat{h} - \hat{1}\right\rangle \\ &\le -\frac{\alpha_1^{\,2}(2l-1)}{2\lambda l\kappa_1}\left\langle \hat{\boldsymbol{\eta}} - \lambda\hat{\boldsymbol{\chi}}, \hat{\boldsymbol{\eta}} - \lambda\hat{\boldsymbol{\chi}}\right\rangle + \frac{\alpha_1^{\,2}l}{2\lambda\kappa_1}\left\langle \hat{\boldsymbol{\eta}}, \hat{\boldsymbol{\eta}}\right\rangle \\ &\quad - \frac{\alpha_2^{\,2}(2l-1)}{2\lambda l\kappa_2}\left\langle \hat{1} - \lambda\hat{h}, \hat{1} - \lambda\hat{h}\right\rangle + \frac{\alpha_2^{\,2}l}{2\lambda\kappa_2}\left\langle \hat{h}, \hat{h}\right\rangle \end{aligned} \tag{46}$$

Substituting Eq. (46) into Eq. (45),

$$\begin{aligned}\dot{V} &\le -\left\langle \hat{\boldsymbol{s}}, \lambda\hat{k}_c \odot \mathrm{sgn}(\hat{\boldsymbol{s}})\right\rangle - \frac{\alpha_1^{\,2}(2l-1)}{2\lambda l\kappa_1}\left\langle \hat{\boldsymbol{\eta}} - \lambda\hat{\boldsymbol{\chi}}, \hat{\boldsymbol{\eta}} - \lambda\hat{\boldsymbol{\chi}}\right\rangle \\ &\quad + \frac{\alpha_1^{\,2}l}{2\lambda\kappa_1}\left\langle \hat{\boldsymbol{\eta}}, \hat{\boldsymbol{\eta}}\right\rangle - \frac{\alpha_2^{\,2}(2l-1)}{2\lambda l\kappa_2}\left\langle \hat{1} - \lambda\hat{h}, \hat{1} - \lambda\hat{h}\right\rangle \\ &\quad + \frac{\alpha_2^{\,2}l}{2\lambda\kappa_2}\left\langle \hat{h}, \hat{h}\right\rangle \\ &\le -\left\langle \hat{\boldsymbol{s}}, \lambda\hat{k}_c \odot \mathrm{sgn}(\hat{\boldsymbol{s}})\right\rangle - \frac{\alpha_1^{\,2}(2l-1)}{2\lambda l\kappa_1}\left\langle \hat{\boldsymbol{\eta}} - \lambda\hat{\boldsymbol{\chi}}, \hat{\boldsymbol{\eta}} - \lambda\hat{\boldsymbol{\chi}}\right\rangle^{\frac{1}{2}} \\ &\quad - \frac{\alpha_2^{\,2}(2l-1)}{2\lambda l\kappa_2}\left\langle \hat{1} - \lambda\hat{h}, \hat{1} - \lambda\hat{h}\right\rangle^{\frac{1}{2}} \\ &\quad + \frac{\alpha_1^{\,2}(2l-1)}{2\lambda l\kappa_1}\left\langle \hat{\boldsymbol{\eta}} - \lambda\hat{\boldsymbol{\chi}}, \hat{\boldsymbol{\eta}} - \lambda\hat{\boldsymbol{\chi}}\right\rangle^{\frac{1}{2}} \\ &\quad - \frac{\alpha_1^{\,2}(2l-1)}{2\lambda l\kappa_1}\left\langle \hat{\boldsymbol{\eta}} - \lambda\hat{\boldsymbol{\chi}}, \hat{\boldsymbol{\eta}} - \lambda\hat{\boldsymbol{\chi}}\right\rangle \\ &\quad + \frac{\alpha_1^{\,2}l}{2\lambda\kappa_1}\left\langle \hat{\boldsymbol{\eta}}, \hat{\boldsymbol{\eta}}\right\rangle + \frac{\alpha_2^{\,2}(2l-1)}{2\lambda l\kappa_2}\left\langle \hat{1} - \lambda\hat{h}, \hat{1} - \lambda\hat{h}\right\rangle^{\frac{1}{2}} \\ &\quad - \frac{\alpha_2^{\,2}(2l-1)}{2\lambda l\kappa_2}\left\langle \hat{1} - \lambda\hat{h}, \hat{1} - \lambda\hat{h}\right\rangle + \frac{\alpha_2^{\,2}l}{2\lambda\kappa_2}\left\langle \hat{h}, \hat{h}\right\rangle \\ &\le -cV^{\frac{1}{2}} + \frac{\alpha_1^{\,2}(2l-1)}{2\lambda l\kappa_1}\left\langle \hat{\boldsymbol{\eta}} - \lambda\hat{\boldsymbol{\chi}}, \hat{\boldsymbol{\eta}} - \lambda\hat{\boldsymbol{\chi}}\right\rangle^{\frac{1}{2}} \\ &\quad - \frac{\alpha_1^{\,2}(2l-1)}{2\lambda l\kappa_1}\left\langle \hat{\boldsymbol{\eta}} - \lambda\hat{\boldsymbol{\chi}}, \hat{\boldsymbol{\eta}} - \lambda\hat{\boldsymbol{\chi}}\right\rangle \\ &\quad + \frac{\alpha_2^{\,2}(2l-1)}{2\lambda l\kappa_2}\left\langle \hat{1} - \lambda\hat{h}, \hat{1} - \lambda\hat{h}\right\rangle^{\frac{1}{2}} \\ &\quad - \frac{\alpha_2^{\,2}(2l-1)}{2\lambda l\kappa_2}\left\langle \hat{1} - \lambda\hat{h}, \hat{1} - \lambda\hat{h}\right\rangle \\ &\quad + \frac{\alpha_1^{\,2}l}{2\lambda\kappa_1}\left\langle \hat{\boldsymbol{\eta}}, \hat{\boldsymbol{\eta}}\right\rangle + \frac{\alpha_2^{\,2}l}{2\lambda\kappa_2}\left\langle \hat{h}, \hat{h}\right\rangle \end{aligned} \tag{47}$$

where

$$\begin{aligned} c &= \min\{\lambda k_c, \lambda k_c^{\circ}, \frac{\alpha_1^{\,2}(2l-1)}{2\lambda l\kappa_1}, \frac{\alpha_2^{\,2}(2l-1)}{2\lambda l\kappa_2}\} \\ &\quad \cdot \min\{\sqrt{2}, \sqrt{2\lambda\kappa_1}, \sqrt{2\lambda\kappa_2}\} \end{aligned}$$

The following two cases are now analyzed.

Case A: If $\langle \hat{\boldsymbol{\eta}} - \lambda \hat{\boldsymbol{\chi}}, \hat{\boldsymbol{\eta}} - \lambda \hat{\boldsymbol{\chi}} \rangle^{\frac{1}{2}} \geq 1$ and $\left\langle \hat{1} - \lambda \hat{h}, \hat{1} - \lambda \hat{h} \right\rangle^{\frac{1}{2}} \geq 1$, then

$$\frac{\alpha_1^{\,2}(2l-1)}{2\lambda l \kappa_1} \langle \hat{\boldsymbol{\eta}} - \lambda \hat{\boldsymbol{\chi}}, \hat{\boldsymbol{\eta}} - \lambda \hat{\boldsymbol{\chi}} \rangle^{\frac{1}{2}} - \frac{\alpha_1^{\,2}(2l-1)}{2\lambda l \kappa_1} \langle \hat{\boldsymbol{\eta}} - \lambda \hat{\boldsymbol{\chi}}, \hat{\boldsymbol{\eta}} - \lambda \hat{\boldsymbol{\chi}} \rangle \leq 0 \tag{48}$$

$$\frac{\alpha_2^{\,2}(2l-1)}{2\lambda l \kappa_2} \left\langle \hat{1} - \lambda \hat{h}, \hat{1} - \lambda \hat{h} \right\rangle^{\frac{1}{2}} - \frac{\alpha_2^{\,2}(2l-1)}{2\lambda l \kappa_2} \left\langle \hat{1} - \lambda \hat{h}, \hat{1} - \lambda \hat{h} \right\rangle \leq 0 \tag{49}$$

Case B: If $\langle \hat{\boldsymbol{\eta}} - \lambda \hat{\boldsymbol{\chi}}, \hat{\boldsymbol{\eta}} - \lambda \hat{\boldsymbol{\chi}} \rangle^{\frac{1}{2}} < 1$ or $\left\langle \hat{1} - \lambda \hat{h}, \hat{1} - \lambda \hat{h} \right\rangle^{\frac{1}{2}} < 1$, then, by completing the square,

$$\frac{\alpha_1^{\,2}(2l-1)}{2\lambda l \kappa_1} \langle \hat{\boldsymbol{\eta}} - \lambda \hat{\boldsymbol{\chi}}, \hat{\boldsymbol{\eta}} - \lambda \hat{\boldsymbol{\chi}} \rangle^{\frac{1}{2}} - \frac{\alpha_1^{\,2}(2l-1)}{2\lambda l \kappa_1} \langle \hat{\boldsymbol{\eta}} - \lambda \hat{\boldsymbol{\chi}}, \hat{\boldsymbol{\eta}} - \lambda \hat{\boldsymbol{\chi}} \rangle \leq \frac{\alpha_1^{\,2}(2l-1)}{8\lambda l \kappa_1} \tag{50}$$

$$\frac{\alpha_2^{\,2}(2l-1)}{2\lambda l \kappa_2} \left\langle \hat{1} - \lambda \hat{h}, \hat{1} - \lambda \hat{h} \right\rangle^{\frac{1}{2}} - \frac{\alpha_2^{\,2}(2l-1)}{2\lambda l \kappa_2} \left\langle \hat{1} - \lambda \hat{h}, \hat{1} - \lambda \hat{h} \right\rangle \leq \frac{\alpha_2^{\,2}(2l-1)}{8\lambda l \kappa_2} \tag{51}$$

Based on these analyses and Eqs. (47), (49) and (51), it follows that

$$\begin{aligned} \dot{V} &\leq -cV^{\frac{1}{2}} + \frac{\alpha_1^{\,2}(2l-1)}{8\lambda l \kappa_1} + \frac{\alpha_2^{\,2}(2l-1)}{8\lambda l \kappa_2} \\ &\quad + \frac{\alpha_2^{\,2} l}{2\lambda \kappa_2} \left\langle \hat{h}, \hat{h} \right\rangle + \frac{\alpha_1^{\,2} l}{2\lambda \kappa_1} \langle \hat{\boldsymbol{\eta}}, \hat{\boldsymbol{\eta}} \rangle \\ &\leq -cV^{\frac{1}{2}} + w \end{aligned} \tag{52}$$

where $w = \frac{\alpha_1^{\,2}(2l-1)}{8\lambda l \kappa_1} + \frac{\alpha_2^{\,2}(2l-1)}{8\lambda l \kappa_2} + \frac{\alpha_2^{\,2} l}{2\lambda \kappa_2} \left\langle \hat{h}, \hat{h} \right\rangle + \frac{\alpha_1^{\,2} l}{2\lambda \kappa_1} \langle \hat{\boldsymbol{\eta}}, \hat{\boldsymbol{\eta}} \rangle$.

For further analysis, the following Lemma is introduced.

Lemma 1 [24]: Consider a system $\dot{\boldsymbol{x}} = f(\boldsymbol{x}, \boldsymbol{u})$ and a Lyapunov candidate $V_1(\boldsymbol{x})$. Suppose there exist scalars $\phi > 0$, $0 < p < 1$ and $0 < \vartheta < \infty$ that satisfy

$$\dot{V}_1 \leq -\phi V_1^{\,p}(x) + \vartheta \tag{53}$$

Then the residual set of the solution of this system is given by

$$V_1 \leq \left(\frac{\vartheta}{\phi(1-\theta)} \right)^{\frac{1}{p}} \quad \forall t \geq T \tag{54}$$

where $T \leq V_1(x_0)^{1-p} / (\phi\theta(1-p))$ is a finite time, $V_1(x_0)$ is the initial value of V_1, and $0 < \theta < 1$. V_1 is called practical finite-time stable.

According to Lemma 1, and based on Eq. (52), one obtains

$$V \leq \left(\frac{w}{c(1-\theta)} \right)^2 \quad \forall t \geq t_m \tag{55}$$

where $t_m = 2V(0)^{0.5} / (c\theta)$, $V(0)$ is the initial value of V, and $0 < \theta < 1$. Notice that by choosing appropriate κ_i and α_i, i=1, 2, the region $\left(w / (c(1-\theta)) \right)^2$ can be arbitrarily small, so that when $t \geq t_m$, we have $\hat{\boldsymbol{s}} \triangleq \hat{\mathbf{0}}$, and the sliding condition holds.

Step 2: $\hat{\boldsymbol{s}}$ is a time-varying sliding manifold, and has the following three properties:

1) For $t > t_f$, $\hat{\boldsymbol{f}}(t) = \mathbf{0} + \varepsilon \mathbf{0}$ and $\dot{\hat{\boldsymbol{\xi}}}_{pt}(t) + k\hat{\boldsymbol{\xi}}_{pt}(t) = \hat{\mathbf{0}}$. This property guarantees the asymptotic stability of the sliding manifold.
2) $\lim_{t \to t_m^-} \hat{\boldsymbol{f}}(t) = \lim_{t \to t_m^+} \hat{\boldsymbol{f}}(t) = \hat{\mathbf{0}}$ and $\lim_{t \to t_f^-} \hat{\boldsymbol{f}}(t) = \lim_{t \to t_f^+} \hat{\boldsymbol{f}}(t) = \hat{\mathbf{0}}$, so that $\hat{\boldsymbol{f}}(t)$ is continuous and $\dot{\hat{\boldsymbol{f}}}(t)$ is bounded. This property is required for the existence of the controller.
3) $\hat{\boldsymbol{f}}(0) = \hat{\boldsymbol{f}}(t_m) = \dot{\hat{\boldsymbol{\xi}}}_{pt}(0) + k\hat{\boldsymbol{\xi}}_{pt}(0)$. Furthermore, since $\hat{\boldsymbol{s}} \triangleq \hat{\mathbf{0}}$, $\forall t \geq t_m$, we have $\dot{\hat{\boldsymbol{\xi}}}_{pt}(t_m) + k\hat{\boldsymbol{\xi}}_{pt}(t_m) = \hat{\boldsymbol{f}}(t_m) = \dot{\hat{\boldsymbol{\xi}}}_{pt}(0) + k\hat{\boldsymbol{\xi}}_{pt}(0)$.

According to Step 1, when $t \geq t_m$, the sliding condition holds. Substituting Eq. (37) into Eq. (38) yields

$$\dot{\hat{\boldsymbol{\xi}}}_{pt} + k\hat{\boldsymbol{\xi}}_{pt} = \hat{\boldsymbol{f}}(t) \quad \text{for} \quad t \geq t_m \tag{56}$$

For $t_m \leq t < t_f$, solving Eq. (56) and using Property 3 of $\hat{\boldsymbol{s}}$, we obtain

$$\hat{\boldsymbol{\xi}}_{pt}(t)=\frac{e^{-k(t-t_m)}}{k}\left(\hat{\boldsymbol{p}}_1-\frac{kp_2\hat{\boldsymbol{p}}_1+\dfrac{\pi}{2(t_f-t_m)}p_4\hat{\boldsymbol{p}}_1}{p_3^{\,2}}+\frac{k\tau\hat{\boldsymbol{p}}_1}{p_3}\right)+\frac{\cos\left(\dfrac{\pi(t-t_m)}{2(t_f-t_m)}\right)p_2\hat{\boldsymbol{p}}_1}{p_3^{\,2}}+\frac{\sin\left(\dfrac{\pi(t-t_m)}{2(t_f-t_m)}\right)p_4\hat{\boldsymbol{p}}_1}{p_3^{\,2}}-\frac{k\tau\hat{\boldsymbol{p}}_1(t-t_m)\cos\left(\dfrac{\pi(t-t_m)}{2(t_f-t_m)}\right)}{p_3}-\frac{\dfrac{\pi}{2(t_f-t_m)}\tau\hat{\boldsymbol{p}}_1(t-t_m)\sin\left(\dfrac{\pi(t-t_m)}{2(t_f-t_m)}\right)}{p_3} \tag{57}$$

where

$$\hat{\boldsymbol{p}}_1=\boldsymbol{p}_1+\varepsilon\boldsymbol{p}_1^{\circ}=\dot{\hat{\boldsymbol{\xi}}}_{pt}(0)+k\hat{\boldsymbol{\xi}}_{pt}(0),$$

$$p_2=k^3+\left(\frac{\pi}{2(t_f-t_m)}\right)^2k+\left(k^2-\left(\frac{\pi}{2(t_f-t_m)}\right)^2\right)\tau,$$

$$p_3=\left(\frac{\pi}{2(t_f-t_m)}\right)^2+k^2,$$

and $p_4=\left(\dfrac{\pi}{2(t_f-t_m)}\right)^3+k^2\dfrac{\pi}{2(t_f-t_m)}+2k\dfrac{\pi}{2(t_f-t_m)}\tau$.

When $t=t_f$, setting $\hat{\boldsymbol{\xi}}_{pt}(t_f)=\hat{\mathbf{0}}$, one gives

$$\frac{e^{-k(t_f-t_m)}}{k}\left(\hat{\boldsymbol{p}}_1-\frac{kp_2\hat{\boldsymbol{p}}_1+\dfrac{\pi}{2(t_f-t_m)}p_4\hat{\boldsymbol{p}}_1}{p_3^{\,2}}+\frac{k\tau\hat{\boldsymbol{p}}_1}{p_3}\right)+\frac{p_4\hat{\boldsymbol{p}}_1}{p_3^{\,2}}-\frac{\pi}{2}\frac{\tau}{p_3}\hat{\boldsymbol{p}}_1=\hat{\mathbf{0}} \tag{58}$$

According to Eq. (58), one can further obtain

$$\frac{e^{-k(t_f-t_m)}}{k}\left(\hat{\boldsymbol{p}}_1-\frac{kp_5\hat{\boldsymbol{p}}_1+\dfrac{\pi}{2(t_f-t_m)}p_6\hat{\boldsymbol{p}}_1}{p_3^{\,2}}\right)+\frac{p_6\hat{\boldsymbol{p}}_1}{p_3^{\,2}}=p_7\tau\hat{\boldsymbol{p}}_1 \tag{59}$$

where

$$p_5=k^3+\left(\frac{\pi}{2(t_f-t_m)}\right)^2k,$$

$$p_6=\left(\frac{\pi}{2(t_f-t_m)}\right)^3+k^2\frac{\pi}{2(t_f-t_m)}, \text{ and}$$

$$p_7=\frac{1}{p_3^{\,2}}e^{-k(t_f-t_m)}\left(k^2-\left(\frac{\pi}{2(t_f-t_m)}\right)^2\right)-e^{-k(t_f-t_m)}\frac{1}{p_3}-2k\frac{\pi}{2(t_f-t_m)}\frac{1}{p_3^{\,2}}+\frac{\pi}{2}\frac{1}{p_3}+\frac{2}{p_3^{\,2}}e^{-k(t_f-t_m)}\left(\frac{\pi}{2(t_f-t_m)}\right)^2$$

Thus choosing τ as

$$\tau=\frac{e^{-k(t_f-t_m)}}{kp_7}\left(1-\frac{kp_5+\dfrac{\pi}{2(t_f-t_m)}p_6}{p_3^{\,2}}\right)+\frac{p_6}{p_3^{\,2}p_7} \tag{60}$$

guarantees that $\hat{\boldsymbol{\xi}}_{pt}(t_f)=\hat{\mathbf{0}}$, and furthermore, since $\hat{\boldsymbol{f}}(t)\equiv\hat{\mathbf{0}}$ for $t\geq t_f$, one can get

$$\dot{\hat{\boldsymbol{\xi}}}_{pt}+k\hat{\boldsymbol{\xi}}_{pt}=\hat{\mathbf{0}} \text{ for } t\geq t_f \tag{61}$$

Finally, it is proved that

$$\hat{\boldsymbol{\xi}}_{pt}\equiv\hat{\mathbf{0}} \text{ for } \forall t\geq t_f \tag{62}$$

Remark 2: The dual-quaternion based Lagrange-like model used in this paper is a 6-DOF coupled model, based on this model, the controller proposed in this paper has the ability to cope with attitude and orbit actuator faults at the same time, and the pursuer spacecraft can track the expected attitude and relative motion synchronously.

Remark 3: To further explain the convergence of the states, Figure 2 illustrates the convergence curve of $\hat{\boldsymbol{s}}$ in a qualitative way. The initial value (point A) of $\hat{\boldsymbol{s}}$ is set to $\hat{\mathbf{0}}$, which ensures the system will not deviate too far from the sliding manifold. Then, under the effectiveness of the proposed control law, when $t=t_m$, the system states can reach the sliding surface (at point B) and the sliding condition holds. The orange dashed lines in Fig. 2 denote the points satisfying $\hat{\boldsymbol{s}}=\hat{\mathbf{0}}$ $(t=t_m)$. Subsequently, due to the influence of $\hat{\boldsymbol{f}}(t)$, the curve approaches zero, and finally reaches point O when $t=t_f$.

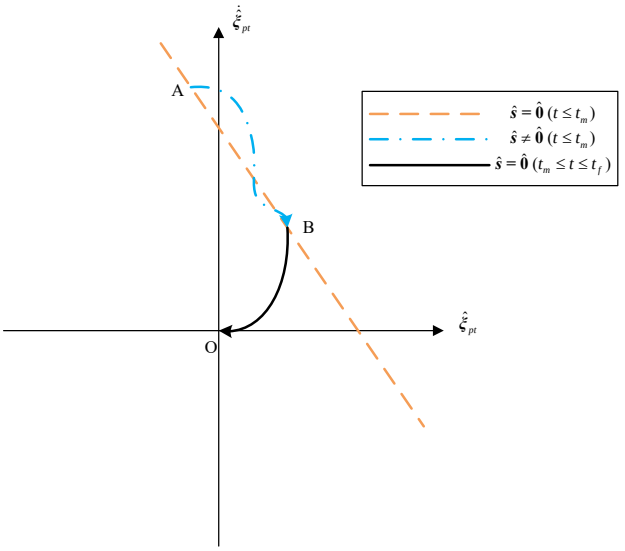

Fig. 2. Convergence of $\hat{s}$

Remark 4: By employing the time-varying sliding manifold, the tracking error of the pursuer is guaranteed to converge to zero within a finite time t_f. A significant advantage of this method is that t_f is explicitly expressed in $\hat{\boldsymbol{f}}(t)$, so that designers can easily change the expected convergence time by changing t_f directly, which is much more convenient than some other finite-time controllers [25, 26] for spacecraft.

Remark 5: One important requirement of the controller is that $\lambda=\min(\lambda_1,\lambda_1^\circ)>0$ ($\hat{\lambda}_1=\lambda_1+\varepsilon\lambda_1^\circ=\lambda_{\min}(\hat{\boldsymbol{A}}\odot\hat{\boldsymbol{H}}(t)\odot\hat{\boldsymbol{A}}^{\mathrm{T}})$). This means that the numbers of actuators n and l (the number of force actuators and torque actuators respectively) should be sufficiently large. Furthermore, since $\hat{\boldsymbol{H}}(t)$ is full-rank, to guarantee $\lambda>0$ there must be at most n-3 attitude actuators and l-3 orbit actuators that have Fault b or Fault d. If $\lambda>0$ cannot be satisfied, then the system is under-actuated, this situation is not considered in this paper.

Remark 6: In Theorem 1, it is explained that by choosing proper control parameters, the convergence domain of V can be arbitrarily small, but this requires the increase of control gains and the extension of t_m. So in practical applications, the designers should balance the accuracy and efficiency of the controller. In the subsequent simulation cases, an appropriate choice of $V(t_m)$, t_m and t_f is identified as $V(t_m)\le 10^{-3}$ and $0.25t_f\le t_m\le 0.5t_f$.

V. Numerical Simulation and Analysis

In this section, by using the 6-DOF spacecraft model proposed in Eq. (31) with the control law and adaptive laws in Eqs. (39)-(41), some numerical simulation results are given and analyzed. The orbital parameters of the target spacecraft are shown in Table I. The main control parameters of the pursuer are shown in Table II.

TABLE I
Parameters of Target's Orbit

Target's orbit parameter	Value
Eccentricity	0.02
Inclination	30°
Longitude ascending node	15°
Semi-major axis	7000 km
Argument of perigee	30°
Initial true anomaly	15°

TABLE II
Other Simulation Parameters

Parameters	Value
m_p	400 kg
$\boldsymbol{J}_p$	[55 1.5 -3 1.5 65 -0.5 -3 -0.5 58] kg·m^2
$\hat{\boldsymbol{\xi}}_{pt}(0)$	[120,-50,80,0.2,-0.2,0.2]$^{\mathrm{T}}$
k	0.1
$\hat{\boldsymbol{\chi}}(0)$	[0.5+ ε 0.5, ε 0.3]$^{\mathrm{T}}$
$\hat{h}(0)$	0.2+ ε 0.2
$\hat{b}_1$	410+ ε 70
$\hat{k}_c$	0.001+ ε 0.005
κ_1	1.5
κ_2	1.5
α_1	0.15
α_2	0.15
θ	0.5

The control objective in this simulation is that the pursuer tracks the attitude of the target, and moves to the expected relative position $p_{pt,d}^p=[15,0,0]$m. The attitude of the target is $[\psi_{t,d},\phi_{t,d},\theta_{t,d}]=[0,\pi\cos(\pi t/180)/6,0]$, where ψ,ϕ,θ denote the yaw, pitch and roll angles respectively. The initial relative quaternion and position between the two spacecraft are $q_{pt}(0)$=[0.4945,0.2483,-0.6187,0.5577] and $p_{pt}^p(0)=[120,-50,80]$m respectively.

In this simulation, the actuators of the pursuer spacecraft are flywheels and thrusters. There are four flywheels totally, and the configuration structure of the flywheels is shown in Fig. 3, three of them along the axes, and the last one is symmetrical with others.

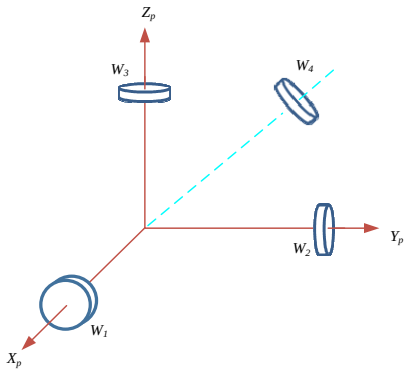

Fig. 3. The configuration of the flywheels

The moment distribution matrix of flywheels is

$$\mathbf{D}_1 = \begin{bmatrix} 1 & 0 & 0 & \sqrt{3}/3 \\ 0 & 1 & 0 & \sqrt{3}/3 \\ 0 & 0 & 1 & \sqrt{3}/3 \end{bmatrix} \tag{63}$$

There are four pairs of thrusters; their configuration is illustrated in Fig. 4. Each pair of thrusters can give thrust in two directions, and the installation directions and positions of each thruster pair are given in Table 3.

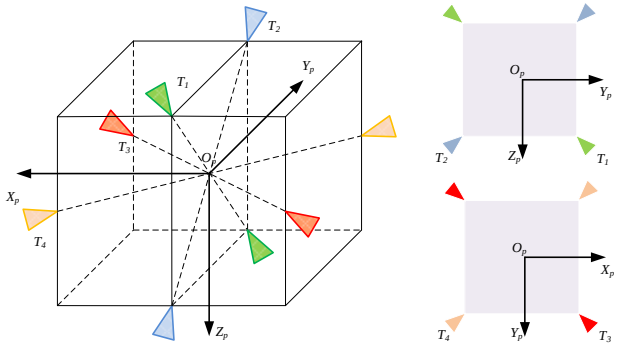

Fig. 4. The configuration structure of thrusters

TABLE III
INSTALLATION DIRECTIONS OF THE THRUSTERS

Thruster Index	Direction
T1	$[0, \sqrt{2}/2, \sqrt{2}/2]$
T2	$[0, -\sqrt{2}/2, \sqrt{2}/2]$
T3	$[\sqrt{2}/2, \sqrt{2}/2, 0]$
T4	$[\sqrt{2}/2, -\sqrt{2}/2, 0]$

From $\mathbf{D}_1$ and Table III, the control allocation matrix $\hat{\boldsymbol{A}}$ can be obtained:

$$\hat{\boldsymbol{A}} = \frac{\sqrt{2}}{2}\begin{bmatrix} 0 & 0 & 1 & 1 \\ 1 & -1 & 1 & -1 \\ 1 & 1 & 0 & 0 \end{bmatrix} + \frac{\varepsilon}{3}\begin{bmatrix} 3 & 0 & 0 & \sqrt{3} \\ 0 & 3 & 0 & \sqrt{3} \\ 0 & 0 & 3 & \sqrt{3} \end{bmatrix} \tag{64}$$

The external disturbance input of the pursuer spacecraft is [27]

$$\begin{aligned} \hat{\boldsymbol{F}}_d^p = {} & 10^{-5} \cdot [-1 \quad 6 \quad -2]^{\mathrm{T}} \sin\left(2\pi\sqrt{\frac{\mu}{r_c^3}}t\right) \mathrm{N} \\ & + \varepsilon 10^{-4} \cdot [1 \quad 2 \quad -2]^{\mathrm{T}} \cos\left(2\pi\sqrt{\frac{\mu}{r_c^3}}t\right) \mathrm{N/m} \end{aligned} \tag{65}$$

where r_c=7000000m is semi-major axis of the target spacecraft.

A. *Simulation for the normal case*

In this case, all of the actuators work normally. Setting t_m=300s and t_f=600s, then the time responses of the relative position and the relative attitude (which has been converted to rotation angle) between the target and the pursuer are shown in Fig. 5. The pursuer does reach the expected position, with the steady error less than 10^{-6}m. Furthermore, the pursuer tracks the attitude of the target with a tracking error less than 10^{-4}rad, and the whole 6-DOF tracking task is accomplished within 600s, as required.

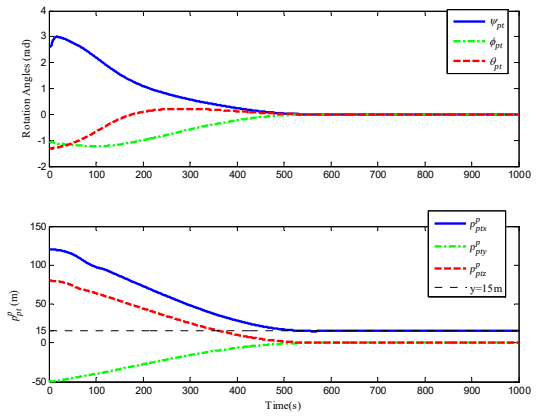

Fig. 5. Time response of states for normal operation

Figure 6 shows the time response of velocity and angular velocity. The tracking error of the dual angle velocity converges to zero within 600s, and then the motion of the two spacecraft is synchronous.

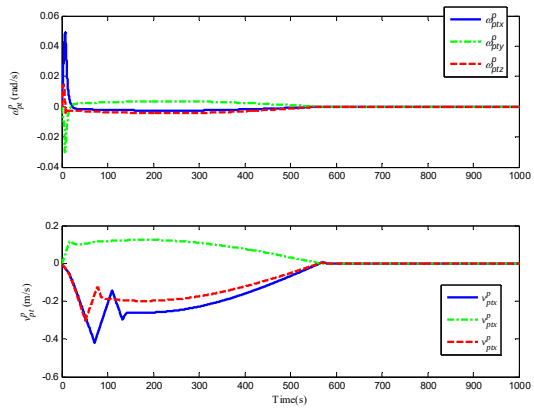

Fig. 6. Time response of relative angle velocity and velocity for normal operation

TABLE IV
SIMULATION PERFORMANCES OF NORMAL CASE

States	Stable errors
Rotation Angles	1×10^{-4} rad
p^p_{pt}	1×10^{-6} m
ω^p_{pt}	2×10^{-6} rad/s
v^p_{pt}	5×10^{-8} m/s

The control outputs of the thrusters and flywheels are given

in Fig. 7 and Fig. 8, which shows that all of the actuators work normally. To summarize, for this simulation case, the proposed control scheme successfully accomplishes target tracking task, the states of the closed-loop system converge to the expected value within the required finite time t_f, and the controller is robust to parameter uncertainties and external disturbances.

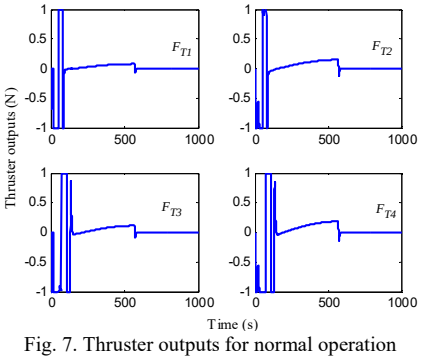

Fig. 7. Thruster outputs for normal operation

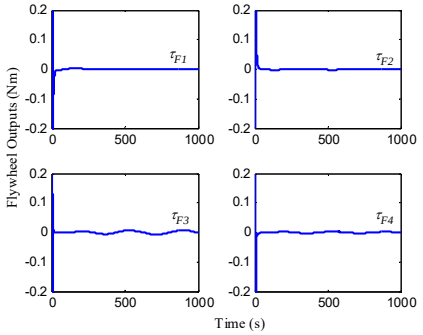

Fig. 8. Flywheel outputs for normal operation

B. *Simulation for the fault case*

In this case, the flywheels and thrusters of the pursuer spacecraft have multiple faults, and the fault-tolerant ability of the controller is illustrated. The fault condition of each actuator is shown in Fig. 9. In this figure, τ_{uci} and F_{ucj} denote the expected outputs of flywheels and thrusters respectively, while τ_{Fi} and F_{Tj} are the real outputs of flywheels and thrusters respectively, with *i=1,2,3,4* and *j=1,2,3,4*. Every actuator has a different kind of fault, and some of them have very serious malfunctions such as complete energy loss and locking. From Fig. 9, the numerical values of $\hat{\boldsymbol{H}}(t)$ and $\hat{\boldsymbol{F}}_f$ can be obtained.

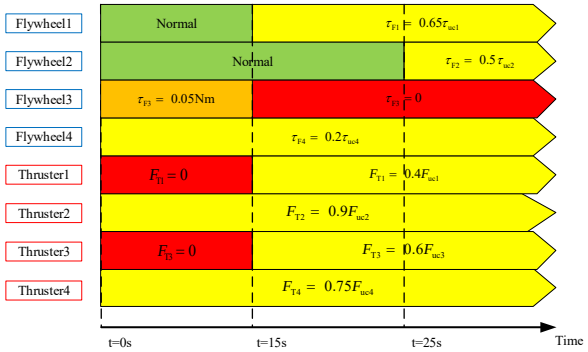

Fig. 9. Fault conditions of actuators

For the actuator fault situation shown in Fig. 9, setting t_m=300s and t_f=600s, Fig. 10 shows the time response of relative positon and relative rotation angle. Although there are some fluctuations caused by the existence of faults, the tracking trajectories still converge within the finite time t_f, and the steady errors of relative position and rotation angle are less than 5×10^{-3} m and 1×10^{-3} rad respectively.

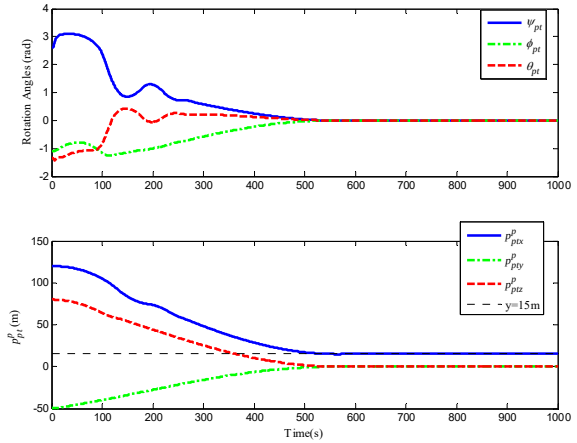

Fig. 10. Time response of states for the faulty actuator case

Figure 11 demonstrates the time responses of relative velocity and angular velocity between the two spacecraft. Due to the existence of actuator faults, the responses are not as smooth as the normal responses shown in Fig. 6. But the control results are similar, and the pursuer can track the motion of the target after 600s.

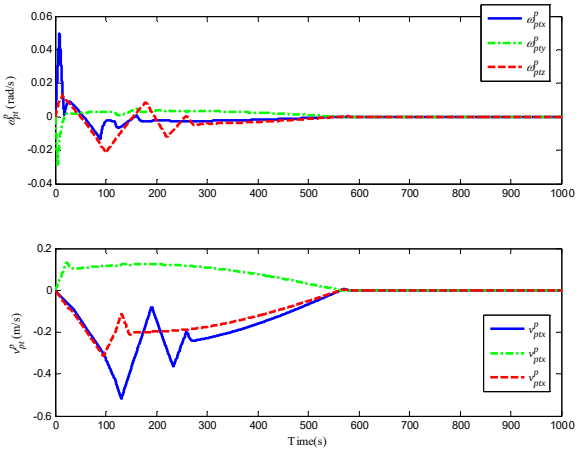

Fig. 11. Time response of velocity for the faulty actuator case

TABLE V
SIMULATION PERFORMANCES OF FAULT CASE

States	Stable errors
Rotation Angles	1×10^{-3} rad
p^p_{pt}	5×10^{-3} m
ω^p_{pt}	1×10^{-5} rad/s
v^p_{pt}	2×10^{-8} m/s

Figures 12 and 13 illustrate the actual outputs of the

actuators. The existence of faults means that some actuators are not functioning properly, and some are not working at all. But the controller still enables the control objective to be achieved.

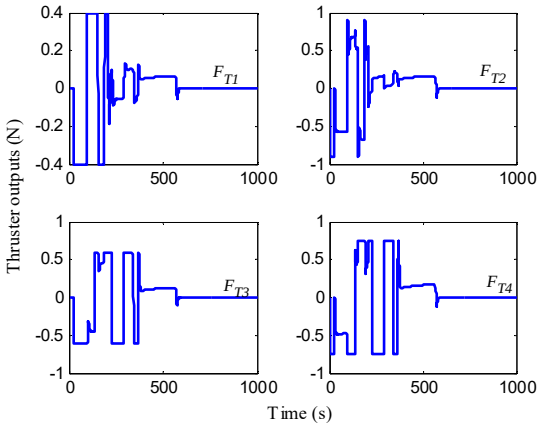

Fig. 12. Thruster outputs for the faulty actuator case

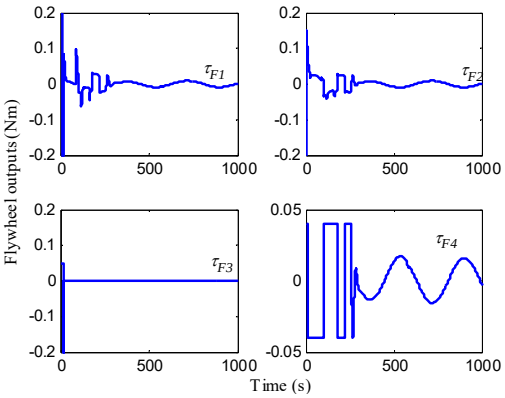

Fig. 13. Flywheel outputs for the faulty actuator case

To demonstrate the finite-time ability of the proposed control law, Figure 14 shows the time responses of relative position and rotation angle when t_f is changed (setting t_m=0.5t_f). The convergence time is different when t_f differs, but it is always less than t_f. This result confirms Theorem 1, and one can design the required convergence time by choosing t_f directly.

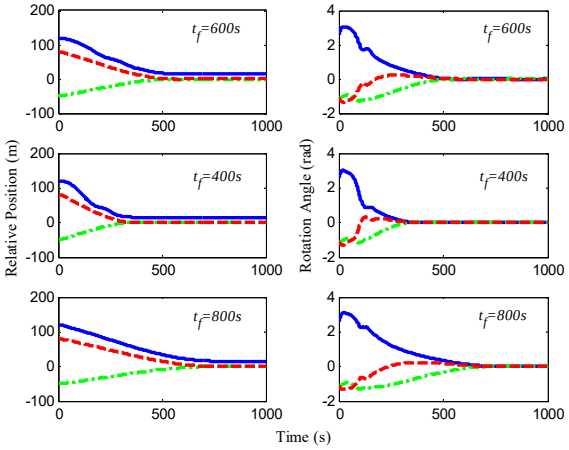

Fig. 14. Time responses of the states for different t_f

To illustrate fault tolerance abilities of the proposed controller, the 3-D trajectories of relative rotation angles and positions are given in Fig. 15 and Fig. 16 respectively. In these two figures, "DFF" denotes the simulation results using the control law proposed in this paper, "ADF" denotes the results using the other adaptive dual-quaternion-based finite-time controller introduced in Ref. [12], and "H-inf" denotes the results using the H∞ controller proposed in Ref. [28]. The results show that though all the three controllers illustrated here can finally stable the system, but "ADF" and "H-inf" only have limited robustness to actuator faults and can't guarantee the tracking accuracy, what's more, the trajectories of "ADF" and "H-inf" can't meet the safety requirements of practical engineering. In contrast, the performance of the presented controller is much better, the precision is improved and the convergence process is shorter and smoother.

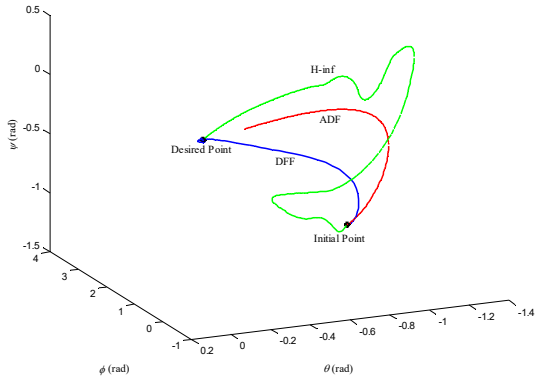

Fig. 15. Trajectories of relative rotation angles

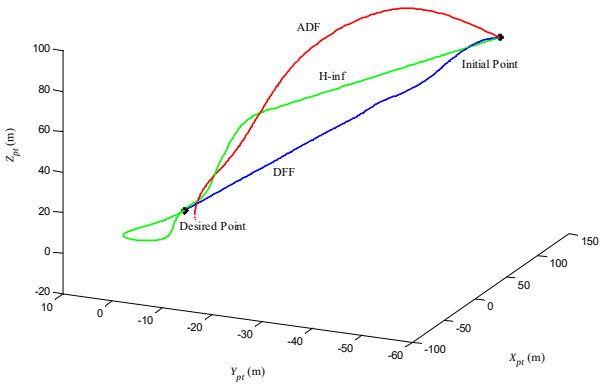

Fig. 16. Trajectories of relative positions

One of the main control objectives is for the pursuer to track the attitude and position of the target synchronously. To illustrate this performance of the proposed controller, let $\Phi = 2\arccos(\eta_{pt})$ denotes the rotation angle between $\mathcal{F}_t$ and $\mathcal{F}_p$, and r_{pt} denotes the desired distance error between centers of mass of the pursuer and the target. Thus Φ can show the convergence of the attitude motion while r_{pt} can demonstrate the approach process of orbit motion. Figure 17 demonstrates the polar curves between Φ and r_{pt}, it shows that comparing with "ADF" and "H-inf", the controller given in this paper has much smoother and better polar trajectory.

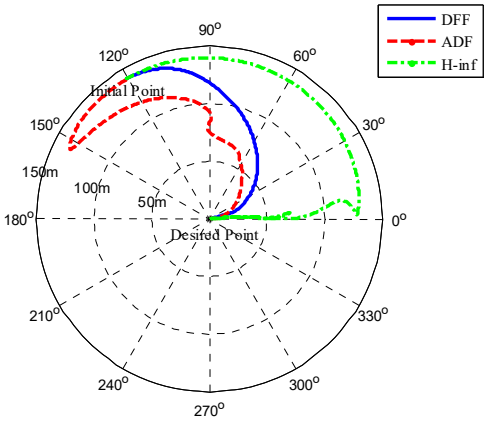

Fig. 17 Polar curves of different controllers

Finally, we use Monte Carlo techniques to evaluate the control method's performance and analyze the worst cases. To proceed the Monte Carlo simulation, first we need to choose the random parameters and their ranges. Since our purpose is to demonstrate the controller's robustness to unknown faults and uncertainties, so the following random parameters are chosen for the simulation:

$$h_i,\ h_i^{\circ} \in [0,1], i = 1,2,3,4 \tag{66}$$

$$F_{fi} \in [-0.02, 0.02]\,\mathrm{N},\ i = 1,2,3,4 \tag{67}$$

$$\tau_{fi} \in [-0.005, 0.005]\,\mathrm{Nm},\ i = 1,2,3,4 \tag{68}$$

$$m_p \in [200, 600]\,\mathrm{kg} \tag{69}$$

$$\boldsymbol{J}_p \in \left\{ \begin{bmatrix} 52 & 1 & -4 \\ 0.5 & 61 & -1.5 \\ -5 & -1.5 & 55 \end{bmatrix} \text{to} \begin{bmatrix} 58 & 2 & -5 \\ 2.5 & 69 & 0.5 \\ -1 & 0.5 & 61 \end{bmatrix} \right\} \mathrm{kg \cdot m^2} \tag{70}$$

The process of a single simulation can be described as: firstly using Monte Carlo techniques to generate a set of new random parameter values as mentioned above, and then simulate the closed-loop system with the generated random values and the fixed control parameters, finally record the final tracking errors of the simulation. The relative attitude tracking errors and relative position tracking errors of 1000 times simulations are shown in Fig. 18 and Fig. 19 respectively. The subfigures in the left of Figs.18 and 19 shows the overall distribution of tracking errors, and the partial enlargements in the right shows the stable part of tracking errors. It can be seen from Figs. 18 and 19 that overwhelming majority of simulations have very good results even though under the unknown actuator faults and uncertainties, and can finally complete the control task with high precision ($\Phi < 1\times10^{-3} rad$, $r_{pt} < 1\times10^{-2} m$).

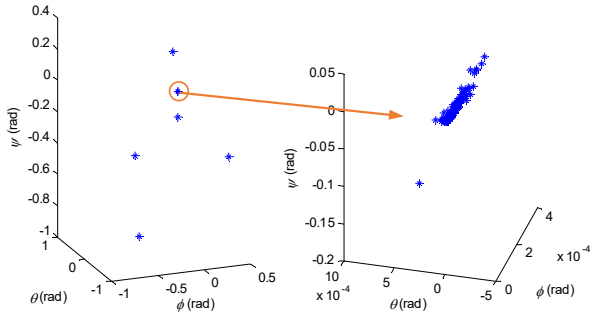

Fig. 18 Relative attitude tracking errors under Monte Carlo simulation

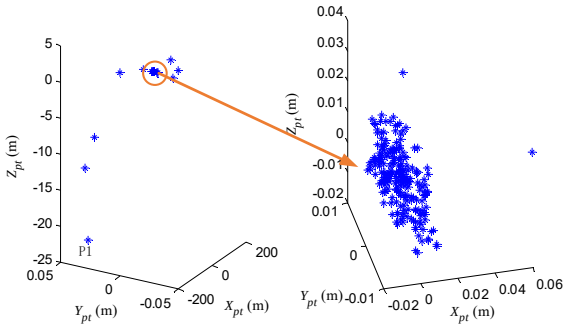

Fig. 19 Relative position tracking errors under Monte Carlo simulation

Then we analyze the few unstable points shown in Figs. 18 and 19 (the points not converge to areas near the origin, which means the corresponding simulations can't meet the control requirements). The conclusion is that these unstable results are caused by underactuation, for example, for the worst case P1 in Fig.19, the real part of its fault matrix is

$$\begin{aligned} \boldsymbol{H}^{p1} &= \mathrm{diag}(h_1^{p1}, h_2^{p2}, h_3^{p3}, h_4^{p4}) \\ &= \begin{bmatrix} 0.0087 & 0 & 0 & 0 \\ 0 & 0.4975 & 0 & 0 \\ 0 & 0 & 0.0149 & 0 \\ 0 & 0 & 0 & 0.8003 \end{bmatrix} \end{aligned} \tag{71}$$

It can be seen from Eq. (71) that, in this case, Thruster 1 and 3 almost can't work, Thruster 2 and 4 can only provide partial actuation to the system, and one can further obtain that:

$$\lambda^{p1} = \lambda_{\min}(\boldsymbol{A}\boldsymbol{H}^{p1}\boldsymbol{A}^{\mathrm{T}}) = 0.0157 \approx 0 \tag{72}$$

Just as we mentioned in **Theorem** 1 and **Remark** 5, the controller proposed in this paper can't handle this situation. In summary, Monte Carlo based simulations shows that the proposed control method has good performance and robustness to hundreds of random actuator faults and uncertainties, and also shows the limitation that our control law can't deal with under-actuated situations.

Summarizing all of the simulation cases, it is noted that by employing the control method proposed in this paper, the

pursuer can accomplish the 6-DOF target tracking task successfully even in the presence of severe actuator faults, external disturbances and parameter uncertainties. In addition, extensive simulations have been performed using different initial values, fault types and controller parameters. Moreover, the flexibility in the choice of convergence time and control parameters can be utilized to obtain the desired performance.

VI. Conclusion

In this paper, a novel fault-tolerant control method is proposed for a target-pursuer spacecraft formation. Specifically, a 6-DOF Lagrange-like model with dual quaternion description is employed to describe the coupled motion between the target and the pursuer. This model is then combined with a novel time-varying sliding manifold, and an adaptive fault-tolerant control law is presented. With the proposed control law, the pursuer can track the 6-DOF motion of the target, and the arrival and convergence to the sliding manifold are proven to occur in finite-time. Furthermore, the proposed control law is robust to external disturbances and parameter uncertainties. Numerical simulation results are given to illustrate the effectiveness and performance of the proposed controller with respect to fast tracking, disturbance suppression, fault tolerance and finite-time stability.

References

[1] A. M. Zou, "Finite-Time Output Feedback Attitude Tracking Control for Rigid Spacecraft," *IEEE T. Contr. Syst. T.*, vol. 22, no. 1, pp. 338-345, Jan, 2014.

[2] A. Taheri, M. A. Shoorehdeli, H. Bahrami, and M. H. Fatehi, "Implementation and Control of X-Y Pedestal Using Dual-Drive Technique and Feedback Error Learning for LEO Satellite Tracking," *IEEE T. Contr. Syst. T.*, vol. 22, no. 4, pp. 1646-1657, Jul, 2014.

[3] D. Lee, and G. Vukovich, "Robust Adaptive Terminal Sliding Mode Control on SE(3) for Autonomous Spacecraft Rendezvous and Docking," *Nonlinear Dynam.*, vol. 83, no. 4, pp. 2263-2279, Mar, 2016.

[4] L. Sun, and W. Huo, "6-DOF Integrated Adaptive Backstepping Control for Spacecraft Proximity Operations," *IEEE T. Aero. Elec. Sys.*, vol. 51, no. 3, pp. 2433-2443, Jul, 2015.

[5] I. Kawano, M. Mokuno, T. Kasai, and T. Suzuki, "Result of Autonomous Rendezvous Docking Experiment of Engineering Test Satellite-VII," *J. Spacecraft Rockets*, vol. 38, no. 1, pp. 105-111, Jan-Feb, 2001.

[6] P. K. C. Wang, F. Y. Hadaegh, and K. Lau, "Synchronized Formation Rotation and Attitude Control of Multiple Free-Flying Spacecraft," *J. Guid. Control Dynam.*, vol. 22, no. 1, pp. 28-35, Jan-Feb, 1999.

[7] R. W. Beard, J. Lawton, and F. Y. Hadaegh, "A Coordination Architecture for Spacecraft Formation Control," *IEEE T. Contr. Syst. T.*, vol. 9, no. 6, pp. 777-790, 2001.

[8] L. Breger, and J. P. How, "Safe Trajectories for Autonomous Rendezvous of Spacecraft," *J. Guid. Control Dynam.*, vol. 31, no. 5, pp. 1478-1489, Sep-Oct, 2008.

[9] T. Der-Ren, V. Coverstone-Carroll, and J. E. Prussing, "Optimal Impulsive Time-Fixed Orbital Rendezvous and Interception with Path Constraints," *J. Guid. Control Dynam.*, vol. 18, no. 1, pp. 54-60, Jan.-Feb., 1995.

[10] D. Zhang, S. Song, and R. Pei, "Safe Guidance for Autonomous Rendezvous and Docking with a Non-Cooperative Target," *AIAA Guidance, Navigation, and Control Conference*, 2010.

[11] Y. Lv, Q. Hu, G. Ma, and J. Zhou, "6 DOF Synchronized Control for Spacecraft Formation Flying with Input Constraint and Parameter Uncertainties," *ISA T.*, vol. 50, no. 4, pp. 573-80, Oct, 2011.

[12] J. Y. Wang, H. Z. Liang, Z. W. Sun, S. J. Zhang, and M. Liu, "Finite-Time Control for Spacecraft Formation with Dual-Number-Based Description," *J. Guid. Control Dynam*, vol. 35, no. 3, pp. 950-962, May-Jun, 2012.

[13] N. Filipe, and P. Tsiotras, "Adaptive Position and Attitude-Tracking Controller for Satellite Proximity Operations Using Dual Quaternions," *J. Guid. Control Dynam*, pp. 1-12, 2014.

[14] B. Robertson, and E. Stoneking, "Satellite GN&C anomaly trends," *26th Annual AAS Rocky Mountain Guidance and Control Conference*, 2003.

[15] W. C. Cai, X. H. Liao, and Y. D. Song, "Indirect Robust Adaptive Fault-Tolerant Control for Attitude Tracking of Spacecraft," *J. Guid. Control Dynam*, vol. 31, no. 5, pp. 1456-1463, Sep-Oct, 2008.

[16] B. Xiao, Q. L. Hu, and Y. M. Zhang, "Adaptive Sliding Mode Fault Tolerant Attitude Tracking Control for Flexible Spacecraft Under Actuator Saturation," *IEEE T. Contr. Syst. T.*, vol. 20, no. 6, pp. 1605-1612, Nov, 2012.

[17] T. Schetter, M. Campbell, and D. Surka, "Multiple Agent-Based Autonomy for Satellite Constellations," *Artif. Intell.*, vol. 145, no. 1-2, pp. 147-180, Apr, 2003.

[18] H. Lee, and Y. Kim, "Fault-Tolerant Control Scheme for Satellite Attitude Control System," *IET Control Theory A.*, vol. 4, no. 8, pp. 1436-1450, Aug, 2010.

[19] Y. S. Lu, and J. S. Chen, "Design of A Global Sliding-Mode Controller for A Motor Drive With Bounded Control," *Int. J. Control*, vol. 62, no. 5, pp. 1001-1019, Nov, 1995.

[20] J. Y. Lin, Y. S. Lu, and J. S. Chen, "A Global Sliding-Mode Control Scheme with Adjustable Robustness for a Linear Variable Reluctance Motor," *JSME Int. J. C-Mech. Sy.*, vol. 45, no. 1, pp. 215-225, Mar, 2002.

[21] W. K. Clifford, "Preliminary Sketch of Bi-Quaternions," *P. Lond. Math. Soc.*, vol. 4, pp. 381-395, 1873.

[22] E. Study, "Von Den Bewegungen und Umlegungen," *Math. Ann.*, vol. 39, no. 4, pp. 441-556, 1891.

[23] S. Murugesan, and P. Goel, "Fault-Tolerant Spacecraft Attitude Control System," *Sadhana*, vol. 11, no. 1-2, pp. 233-261, Oct, 1987.

[24] Z. Man, A. P. Paplinski, and H. R. Wu, "A Robust MIMO Terminal Sliding Mode Control Scheme for Rigid Robotic Manipulators," *IEEE T. Automat. Contr*, vol. 39, no. 12, pp. 2464-2469, Dec., 1994.

[25] H. B. Du, S. H. Li, and C. J. Qian, "Finite-Time Attitude Tracking Control of Spacecraft With Application to Attitude Synchronization," *IEEE T. Automat. Contr*, vol. 56, no. 11, pp. 2711-2717, Nov, 2011.

[26] Z. Zhu, Y. Q. Xia, and M. Y. Fu, "Attitude Stabilization of Rigid Spacecraft with Finite-Time Convergence," *Int. J. Robust. Nonlin.*, vol. 21, no. 6, pp. 686-702, Apr, 2011.

[27] S. N. Singh, "Adaptive Output Feedback Spacecraft Formation Flying Via Observer Based Feedback Linearization," *51st AIAA Aerospace Sciences Meeting Including the New Horizons Forum & Aerospace Exposition*, 2013.

[28] Y. Ikeda, T. Kida, and T. Nagashio, "Nonlinear Tracking Control of Rigid Spacecraft Under Disturbance Using PD and PID Type $H\infty$ State Feedback," pp. 6184-6191. *50th IEEE Conference on Decision and Control and European Control Conference*, pp. 6184-6191, 2011.

[29] S. S. D. Xu, C. C. Chen, and Z. L. Wu, "Study of Nonsingular Fast Terminal Sliding-Mode Fault-Tolerant Control," *IEEE T. Ind. electron*, vol. 62, no. 6, pp. 3906-3913, Jun, 2015.

[30] J. Q. Li, and K. D. Kumar, "Decentralized Fault-Tolerant Control for Satellite Attitude Synchronization," *IEEE T. Fuzzy Syst.*, vol. 20, no. 3, pp. 572-586, Jun, 2012.

[31] Q. Song, and Y. D. Song, "Data-Based Fault-Tolerant Control of High-Speed Trains with Traction/Braking Notch Nonlinearities and Actuator Failures," *IEEE T. Neural. Networ.*, vol. 22, no. 12, pp. 2250-2261, Dec, 2011.

[32] Q. L. Hu, H. Y. Dong, Y. M. Zhang, and G. F. Ma, "Tracking Control of Spacecraft Formation Flying with Collision Avoidance," *Aerosp. Sci. and Technol.*, vol. 42, pp. 353-364, Apr-May, 2015.

[33] Z. Y. Meng, W. Ren, and Z. You, "Distributed Finite-Time Attitude Containment Control for Multiple Rigid Bodies," *Automatica*, vol. 46, no. 12, pp. 2092-2099, Dec, 2010.

[34] Y. J. Xu, "Chattering Free Robust Control for Nonlinear Systems," *IEEE T. Contr. Syst. T.*, vol. 16, no. 6, pp. 1352-1359, Nov, 2008.

[35] J. Y. Wang, and Z. W. Sun, "6-DOF Robust Adaptive Terminal Sliding Mode Control for Spacecraft Formation Flying," *Acta Astronaut.*, vol. 73, pp. 76-87, Apr-May, 2012.

[36] A. M. Zou, and K. D. Kumar, "Distributed Attitude Coordination Control for Spacecraft Formation Flying," *IEEE T. Aero. Elec. Sys.*, vol. 48, no. 2, pp. 1329-1346, Apr, 2012.